A High Statistics Study of States Containing Heavy Quarks Using the Wideband Photon Beam and the E687 Multiparticle Spectrometer

Submitted by the Wideband Beam Photon Collaboration

S. Bianco, P. Frabetti, A. Zallo, Dip. di Fisica dell'Universita' and INFN - Bologna, I-40126 Bologna, Italy

V. Paolone, P.M. Yager, University of California-Davis, Davis, CA 95616, USA

H. Cheung,J. Ginkel,V.S. Greene, J. Cumalat, University of Colorado, Boulder, CO 80309, USA

J. Butler,L. Gaines,P.H. Garbincius, L. Garren, S. Gourlay,D.J. Harding, P. Kasper, A. Kreymer, P. Lebrun, S. Shukla, Fermilab, Batavia, IL 60510, USA

S. Bianco, F. Fabbri, A. Zallo, Laboratori Nazionali di Frascati, I-00044 Frascati, Italy

R.W. Gardner, J. Wiss, University of Illinois at Urbana-Champaign, Urbana,IL 61801

J.S. Kang, Korea University, Seoul 136-701, Korea

G. Alimonti, G. Bellini, M. Di Corato, G. Giammarchi, F. Levarato, D. Menasce, E. Meroni, L. Moroni, D. Pedrini,L. Perasso,S. Sala, Dip. di Fisica dell'Universita' and INFN - Milano, I-20133 Milan, Italy

F. Davenport, University of North Carolina-Asheville, Ashville, NC 28804, USA

J.F. Filaseta, Northern Kentucky University, Highland Heights, KY 41076, USA

W. Shephard, University of Notre Dame, Notre Dame, IN 46556, USA

V. Arena, G. Boca, C. Castoldi, S. Ratti, P. Vitulo, Dip. di Fisica dell'Universita' and INFN - Pavia, I-27100 Pavia, Italy

A. Lopes, University of Puerto Rico at Mayaguez, Puerto Rico

J. Wilson, University of South Carolina

W. M. Bugg, G.T. Condo, T. Handler, University of Tennessee, Knoxville, TN 37996, USA

P. Sheldon, Vanderbilt University, Nashville, TN 37235, USA

September 1, 1992

Abstract

The spectrometer used in Fermilab Experiment 687 to study the photoproduction and decay of charmed particles will be upgraded to enable it to accumulate 10^6 fully reconstructed charm particles. The physics will involve high precision studies of the D semileptonic decays, QCD studies of Double D events, a measurement of the absolute branching fraction for the D^0, searches for D^0 mixing, CP violation, rare and forbidden decays, fully leptonic decays of the D^+ and a systematic investigation of charm baryons and their lifetimes.

A High Statistics Study of States Containing Heavy Quarks Using the Wideband Photon Beam and the E687 Multiparticle Spectrometer

Submitted by the Wideband Beam Photon Collaboration

September 1, 1992

Summary

The spectrometer used in Fermilab Experiment 687 to study the photoproduction and decay of charmed particles will be upgraded to enable it to accumulate 10^6 fully reconstructed charm particles. The physics will involve high precision studies of the D semileptonic decays, QCD studies of Double D events, a measurement of the absolute branching fraction for the D^0, searches for D^0 mixing, CP violation, rare and forbidden decays, fully leptonic decays of the D^+ and a systematic investigation of charm baryons and their lifetimes. The estimates of charm yields are based on reasonable extrapolations from channels we have already studied in E687.

The increased yield of charm will be obtained by 1) running at over 5 times the average luminosity of E-687 and 2) increasing the efficiency of the detector by a factor of 2. The increased luminosity will be achieved by lowering the beam energy to 250 GeV, using the positron arm of the beam, running at higher average proton intensity, and (hopefully) employing 900 GeV incident protons. Additional gains can come from using a thicker radiator and/or a thicker target.

The detector must be upgraded to handle the increased luminosity. Major changes are:

1. Speeding up the Hadron Calorimeter and using it in the First Level Trigger to reduce deadtime,
2. Improving the time response of the vertex Microstrip Detector,
3. Deadening the PWCs in the beam region and adding straw tube planes to cover the deadened regions. The straw tubes will, in fact, cover the whole aperture, thereby improving tracking over the entire spectrometer,
4. Speeding up the Front End Electronics by a factor of 10,
5. Speeding up the Data Acquisition System, and
6. Improving the Second Level Trigger.

Additional changes will be made to the Muon system, the Cerenkov system, and the Electromagnetic Calorimeters. The Photon Energy Tagging represents a very difficult problem, which is discussed at length. The energy tagging is necessary for the study of production dynamics.

The purpose of Fermilab Experiment 687 is to study the production and decay of charm and beauty particles using a high intensity, high energy photon beam, the Fermilab Wideband Photon Beam. The E687 spectrometer is shown in Figure 1. E687 finished datataking in January 1992. By the middle of August, 1992 all our data was reconstructed. Results from half the data sample are now being discussed and have been presented at conferences. One result on the observation of a charm-doubly strange baryon, Ω_c^0, is being readied for publication.

Some of the highlights of our results thus far are a large sample of semileptonic decays which lead to the best value for the CKM matrix element $|V_{cs}|$, observation of new charm baryon decay channels, measurement of the lifetimes for four charm baryons, observation of a large sample of $D - \overline{D}$ events, demonstration of our ability to measure absolute branching ratios for the D^0, Dalitz plot analysis for several modes, and setting the best limits for $D^0 - \overline{D^0}$ mixing and direct CP violation in the charm sector.

The history of E687 is as follows. We have had three distinct running periods. In each period we have made changes and improved the quality of the data. In the first running period, from June 1987 to February 1988, a sample of about 10,000 fully reconstructed charm particles was obtained. In the second running period, from February to August 1990, about 5 times more data was collected. In the third running period from June 1991 to January 1992 an equal sample to the second running period was obtained. The second and third running periods form a dataset containing 100,000 fully reconstructed charm particles decaying into all charged final states (including those with neutral vees) and a large sample of states with π^0's. These charm particles allow us to explore charm spectroscopy at a level never before achieved.

As we look towards the future we believe that we are able to increase our yield of charm particles yet another order of magnitude. The increased statistics will allow us to improve many programmatic measurements and push limits or hopefully observe signals on topics which would indicate new physics. We believe our principal competition will be from CLEO and possibly from other fixed target experiments. The cleanliness of our signals and the ability to accurately measure particles' lifetimes make this experiment unique. We believe that we understand the dynamics of photoproduction and the large samples already in hand allow us to predict with confidence what we can achieve. Our goal has been set to obtain a sample of about one million fully reconstructed charm particles, which is one order of magnitude higher than that obtained in the current run of E687.

This document is organized as follows: Section 1 presents the physics motivation for obtaining a very large sample of charm particles; Section 2 presents method for achieving the higher photon fluxes; Section 3 describes the modifications and upgrades to the spectrometer that are needed to handle the higher intensity (this includes a discussion of changes to the detector, data-acquistion system, and trigger); Section 4 describes additional possible upgrades that will

improve the overall efficiency for reconstructing charm decays; Section 5 presents estimates of the computer resources required for offline analysis of this large dataset; Section 6 explains the beam request and running conditions for the experiment. In some cases, in this document, we list several options or possible approaches to a technical problem. It should be noted that each technical problem whose solution is essential for the success of the experiment has at least one solution that will definitely work and that can be implemented at reasonable cost.

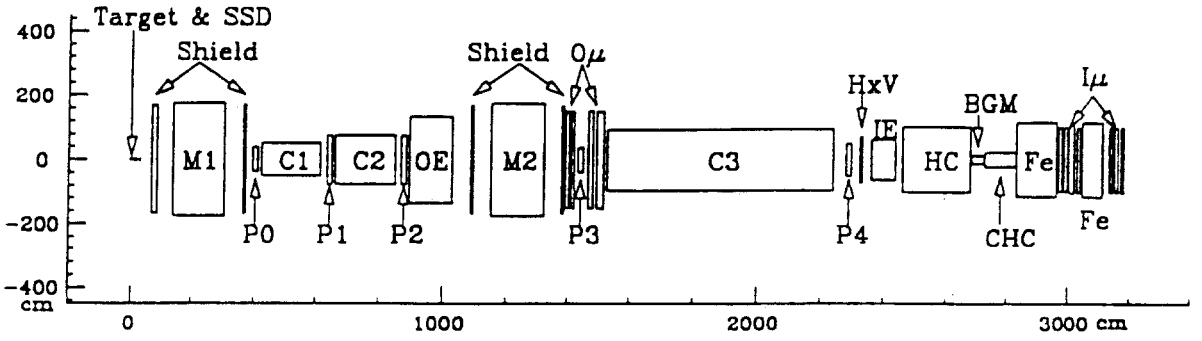

Top View

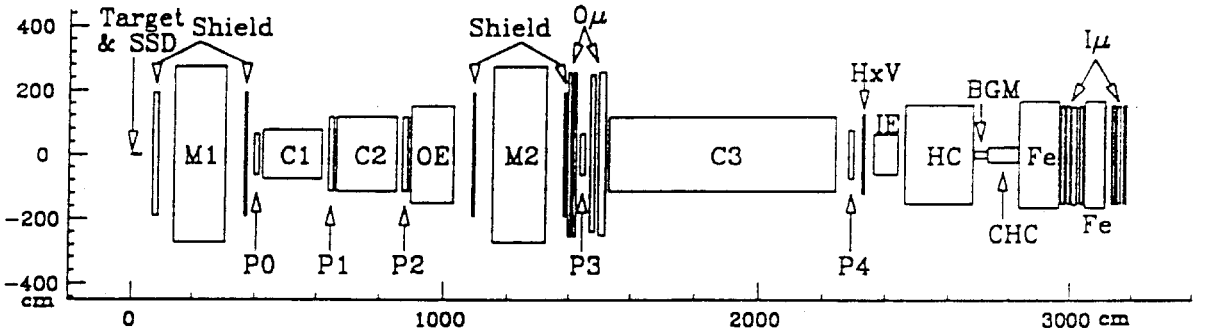

Side View

Figure 1: Schematic representation of E687 spectrometer

1 Motivation for a High Luminosity Investigation of Heavy Flavors

The subject of charm spectroscopy is now 15 years old. However, there are still many areas in which our knowledge is rather limited. Information has been accumulated slowly because of the complexity of the final states, the smallness of the cross sections, the small size of the branching fractions, and the large backgrounds. A major goal of the experiment proposed here is to investigate the open issues in the standard model of charm spectroscopy. For example, this experiment is unique in its ability to study charmed baryons, and should be a major contributor to the study of D^0-$\bar{D}^0$ mixing and semileptonic decays. These and other "programmatic" studies are discussed below. We also list areas where it is possible to search for new physics, beyond the standard model. These searches will emerge as a by-product of the programmatic investigations and will be referred to, following I. Bigi[1], as High Impact Physics studies.

1.1 Programmatic Investigations of Charm

1.1.1 D^0-$\bar{D}^0$ Mixing and Doubly-Suppressed Cabibbo Decays

In the Standard Model, the classic mechanism for mixing is the box-diagram. Predictions for D^0-$\bar{D}^0$ mixing are tiny[2], of order 10^{-6}, and would be unobservable by any existing or projected experiment. However, it has been observed that, for the charm quark, the box-diagram that contributes most involves light quarks — s and d. As a result, long distance effects could be important, and final state interactions may have to be taken into account[3]. A recent calculation, which maintains a relatively close contact with existing measurements, predicts a mixing parameter r of 5×10^{-3}[4]. Mixing at this level will be measureable in the proposed experiment.

D^0-$\bar{D}^0$ Mixing is studied in the experiment by examining the ratio

$$r = \frac{(D^{*+} \rightarrow D^0\pi^+ \rightarrow (K^+\pi^-)\pi^+}{(D^{*+} \rightarrow D^0\pi^+ \rightarrow (K^-\pi^+)\pi^+} = \frac{WS}{RS} \tag{1}$$

in absence of all backgrounds we can parameterize the right sign,(RS), and the wrong sign, (WS), signals as

$$RS(t) = n\ f(t)\ \frac{e^{-t/\tau_D}}{\tau_D} \tag{2}$$

and

$$WS(t) \approx r\ n\ f(t)\frac{t^2 e^{-t/\tau_D}}{2\tau_D^3} + DCSD\ f(t)\frac{e^{-t/\tau_D}}{\tau_D} \tag{3}$$

where $f(t)$ is a Monte Carlo efficiency correction as a function of t, n is the number of right sign events, and τ_D is the lifetime of the D^0 meson.

Using data from the 1988 run and a portion of the 1990 run E687 has obtained a limit of r < 0.0034 at 90% CL. This is slightly better than the previous limit of E691. Presuming that we are able to understand the backgrounds the limit could be lowered to at least r< 0.001 at 90% CL using the existing E687 data. With this experiment we would certainly improve the World Limit another factor of $\sqrt{10}$ and it might be possible to achieve a factor of 10 or even observe mixing. Our sensitivity should be below the theoretical limit mentioned above[4] of 0.0005.

The associated topic of doubly-suppressed Cabibbo decays will also be addressed. These decays have branching fractions relative to the allowed decays of $tan^4(\theta_c)$ and should occur at roughly the 0.25×10^{-2} level. E691 recently published a possible observation of the doubly-suppressed decay $D^+ \rightarrow \phi K^+$. If this is a real signal, then E687 should have possibly 50 such decays and this experiment should have several hundred decays. In E687 we have also searched for a doubly-supressed decay of $D^+ \rightarrow K^+\pi^-\pi^+$ obtained a limit of $\frac{\Gamma(D^+ \rightarrow K^+\pi^-\pi^+)}{\Gamma(D^+ \rightarrow K^-\pi^+\pi^+)} < 0.01$ at the 90%CL. The best previous limit is from Mark I and is 5 times larger. This experiment should observe several doubly-suppressed Cabbibo decay channels.

1.1.2 Semileptonic Decays

Semileptonic decays are interesting because they are easier to interpret theoretically than hadronic decays. There are several important measurements to be made. From measurements of semileptonic branching ratios, the proposed experiment could determine the CKM matrix element $|V_{cs}|$ to 2% and the ratio of elements $|V_{cs}|/|V_{cd}|$ to 4%. In fact, the measurements of this experiment are likely to be limited by theoretical and systematic errors. The form factors for the D^0, D^+, and the D_s^+ mesons will be determined. An interesting theoretical advance by Isgur and Wise[5] shows that measurements of charm form factors can be used to predict beauty form factors. The polarization of the W in D^0 , D^+ , and D_s^+ decays will be measured, and interference effects, such as those between the $K^*(890)$ and $K^*(1440)$, will also be investigated. Finally, it will be possible to study the semileptonic decays of charm baryons.

The accuracy to which such determinations of the weak mixing parameters can be made depends on the correctness of the theoretical models used to calculate weak current mixing elements. These models will be improved as better data becomes available. In a recent review article[6] of charm mesons the largest deviation from the Standard Model was claimed to be the ratio of $D \rightarrow K^*e^+\nu$ to $D \rightarrow Ke^+\nu$. The accuracy of course also depends on the experimental statistical and systematic errors.

First we address the issue of how well the CKM, $|V_{cs}|$ and $|V_{cd}|$ can be determined through the decays of charm particles. Historically, $|V_{cd}|$, has been obtained from neutrino and anti-neutrino measurements off valence d quarks. The best measurement[7] determines $|V_{cd}| = 0.21 \pm 0.03$. This measurement is

Table 1: Selected Semileptonic Decays

Mode	Branch Ratio (%)	Exp.
$D^0 \to e^+X$	7.5±1.1±0.4	MkIII[9]
$D^+ \to e^+X$	17.0±1.9±0.7	MkIII[9]
$D^0 \to K^-e^+\nu_e$	3.8±0.5±0.6	E691[13]
	3.4±0.5±0.4	MkIII[10]
	3.8±0.3±0.6	CLEO[12]
	3.9±0.2±0.7	ARGUS[6]
$D^0 \to K^-\mu^+\nu_\mu$	2.5±0.4±0.5	E653[11]
$D^0 \to \pi^-e^+\nu_e$	$0.39^{+0.23}_{-0.11}$±0.04	MkIII[9]

Table 2: Number of D^0 Reconstructed Decays

Decay Channel	Br	Events	CKM Element
$K^-l^+\nu$	0.034	10,000	$\|V_{cs}\|$
$\pi^-l^+\nu$	0.004	1200	$\|V_{cd}\|$
$K^{*-}l^+\nu$	0.06	1000	$\|V_{cs}\|$
$\rho^-l^+\nu$	0.004	600	$\|V_{cd}\|$

dependent on the production cross section for D^0 and D^+ charm mesons. The measurement is further dependent on the semileptonic branching ratios and the fragmentation function of each charm particle.

Table 1 lists some of the semileptonic decay channels which have been detected. The inclusive D measurements are determined by Mark III[9]. The result from E653[11] uses an inclusive branching fraction of $D^0 \to e^+X = 7.7\pm1.1\%$ and a D^0 lifetime measurement of $(4.28\pm0.11)\times10^{-13}$sec. As can be seen there is much work to be done.

In table 2 we present the estimated number of events we will accumulate in this experiment.

In figure 2 we present a signal for $D^0 \to K^-\mu\nu$ from a partial sample of E687 data. It is clear that a remarkably clean signal is observed. E687 measures the ratio $\Gamma(D^0 \to K^-e^+\nu_e)/\Gamma(D^0 \to K^-\pi^+)$ and could use the Mark III branching fraction[9] of $B(D^0 \to K^-\pi^+) = (4.2\pm0.4\pm0.4)\%$ to obtain their measurement of the absolute branching fraction. In addition, the D^0 lifetime is used to determine the semileptonic partial rate $\Gamma(D^0 \to K^-e^+\nu_e)$. Finally, the partial width is related to the matrix element and form factor as follows: $\Gamma(D^0 \to K^-e^+\nu_e) = |V_{cs}|^2|f_+(0)|^2 1.82\times\ 10^{10}s^{-1}$. where $|f_+(0)|$ is the form factor evaluated at the four-momentum transfer t equal to zero.

Thus we see that in order to measure matrix element $|V_{cs}|$ to the 2% level, four values need to be determined to better than 2%. First, sufficient number of events must be obtained in the channel $D^0 \to K^-e^+\nu_e$. This factor is accom-

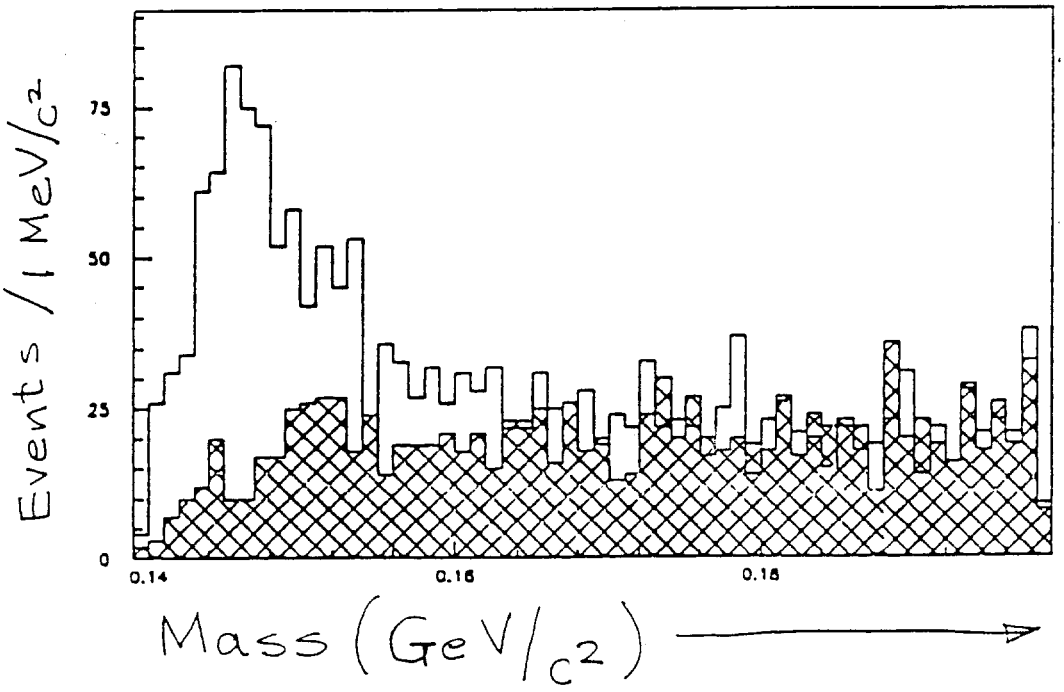

Figure 2 Mass Difference of D^{*+} -D^0 with $D^0 \rightarrow K^- \mu \nu$. The hatched section of the plot is for wrong sign soft pion events.

plished with 10,000 events. Second, the D^0 lifetime needs to be determined to to about the 1% level. This requirement also poses no difficulty as the lifetime is presently measured to 2.5% and E687 will measure it better than 1% by the time this experiment is run. Third, theory is imposed to calculate the form factor. More data can be used to show that the form factor follows a single pole description, but more input from theory is needed here. Fourth, the absolute branching fraction has to be determined to better than 2%. Presently, it is only measured to 10%. A better value is required. E687 will measure the absolute branching fraction to better than 7%. This experiment will attempt to measure the absolute branching fraction to 2%. (See section 1.2.1)

A measurement which is independent of a precise determination of absolute branching fraction is the relative measurement of RAT, where $RAT = \Gamma(D^0 \rightarrow \pi^- e^+ \nu_e)/\Gamma(D^0 \rightarrow K^- e^+ \nu_e)$. Hence we can extract

$$|V_{cd}/V_{cs}|^2 = RAT \times (f_+^K(0)/(f_+^\pi(0))^2 \tag{4}$$

The statistical uncertainty is such that the value of RAT will be known to about 4%. The major uncertainty will be how well the form factors can be determined. A significant systematic uncertainty may also be how well the $D^0 \rightarrow \pi^- e^+ \nu_e$ decay can be identified. There is background from $D^0 \rightarrow K^{*-} e^+ \nu_e$ when the K^0 is missing and also from $D^0 \rightarrow \rho^- e^+ \nu_e$ when the π^0 is missing from the ρ^- decay; however both states will be independently measured so that an accurate subtraction is made.

1.1.3 f_D – the Pseudoscalar Decay Constant

The simplest of all weak decays are the pure leptonic decays of charmed mesons. The decay probability is in principle well described by the standard model of weak interaction as

$$\Gamma(D^+ \rightarrow l^+ \nu_l) = \frac{G_F^2}{8\pi} f_D^2 \; m_D \; m_l^2 |v_{cd}|^2 (1 - \frac{m_l^2}{m_D^2})^2 \tag{5}$$

If the fully leptonic decay of the D_s^+ is calculated, then the $|V_{cs}|$ is substituted for $|V_{cd}|$ and the D_s^+ mass is substituted for the D^+ mass. In the formula, G_F is the well known fermi coupling constant, m_D is the mass of either the D^+ or the D_s^+, m_l is the mass of the lepton, and $|V_{cd}|$ & $|V_{cs}|$ are CKM matrix elements. The value f_D describes the effect of the strong interaction on the charm meson-W coupling.

The weak decay constant has been calculated by several theorists with results that f_D is about 200 MeV and and f_{D_s} is slightly larger around 230 MeV. By measuring the leptonic branching fraction and by knowledge of the D meson lifetime and the CKM matrix elements $|V_{cs}|$ and $|V_{cd}|$, the weak decay constants of the D mesons can be determined experimentally. At this time no experimental measurement of the weak decay constants exists; however, MARK III has set an upper limit for f_D of 290 MeV.

Table 3: Calculated Leptonic Branching Fractions

Decay	Rate (sec^{-1})	Branching Ratio
$D^+ \rightarrow \tau^+\nu_\tau$	8.5×10^8	8.8×10^{-4}
$D^+ \rightarrow \mu^+\nu_\mu$	3.3×10^8	3.5×10^{-4}
$D^+ \rightarrow e^+\nu_e$	7.6×10^3	7.9×10^{-9}
$D_s^+ \rightarrow \tau^+\nu_\tau$	8.6×10^{10}	3.8×10^{-2}
$D_s^+ \rightarrow \mu^+\nu_\mu$	9.0×10^9	4.0×10^{-3}
$D_s^+ \rightarrow e^+\nu_e$	2.0×10^5	9.0×10^{-8}

The table below displays the calculated leptonic decay rate and the expected branching fractions assuming $f_D = 200\ MeV$ and $f_{D_s} = 230\ MeV$, and with $|V_{cd}| = 0.22$ and $|V_{cs}| = 0.97$. The April 1990 Particle Data Book lifetime values for the D^+ and D_s^+ are used to compute the branching ratio values.

Due to the V-A structure of the weak interaction, the electron decay of the D mesons is very small. The muon decay channel is also helicity suppressed relative to the τ decay, but due to the limited available phase space it is not suppressed by as much as one might have guessed. It is also worth noting that the $D_s^+ \rightarrow \tau\nu_\tau$ branching ratio is 40 times larger the same mode for the D^+, *but* the $D_s^+ \rightarrow \mu\nu_\mu$ branching ratio is only 10 times larger than that decay channel of the D^+. When the relative production of the D^+ to the D_s^+ is considered, then the fully leptonic decay rate to muons is found to be roughly equal in our experiment for both the D^+ and the D_s^+. The fully leptonic decay to τ leptons is still dominated by the D_s^+ decays.

From the above discussion it is obvious that in order to measure fully leptonic branching fractions, one has to be able to separate D^+ from D_s^+ decays.

Since the branching fractions are so small, the background channels have to be carefully examined. Clearly, the largest background contamination to the fully leptonic decays will be from semileptonic decays. In fact, the semileptonic branching fractions are much larger than the fully leptonic branching fractions.

With enough statistics it should be possible to obtain a signal of $D \rightarrow \mu^+\nu_\mu$ inclusively. This would be accomplished by taking all muons and electrons which miss the primary vertex. By subtracting the "missed" electron yield from the "missed" muon yield, there should leave an excess of desired muons. However, because the semileptonic decay rate is 20-200 times larger than the fully leptonic decay rate this is impractical. A much better technique is required.

We have investigated in Monte Carlo the use of the well known $D^{+*} - D^+$ mass difference. Specifically, we use $D^{*+} \rightarrow \pi^0 D^+$ and begin by reconstructing the π^0 and by identifying a muon which is detached from the primary vertex. By requiring a pizero from the $D* - D$ decay, the D_s^+ **decays are eliminated.** We are presently still studying this channel in the E687 data. We have been investigating 5 variables which aid in isolating $D^+ \rightarrow \mu\nu_\mu$ decay channel. These variables are the energy of the muon, the transverse momentum of the muon

Table 4: D** Status

State	Channel	Mass	Width	Exp.
$D_1(2420)^0$	$D^{*+}\pi^-$	2428±3±2	20	CLEO[18]
		2414±2±5	23	ARGUS[19]
		2428±8±5	13	E691[17]
$D_J(2440)^+$	$D^{*0}\pi^+$	2443±7±5	41	E691[17]
$D_2(2460)^0$	$D^{*+}\pi^-$	2461±3±1	20	CLEO[18]
		2455±3±5	15	ARGUS[20]
		2459±3±2	20	E691[17]
$D_J(2470)^+$	$D^0\pi^+$	2469±4±6	23	ARGUS[21]
$D_{s1}(2536)^+$	$D^{*+}K^0$	2536.6±0.7±0.4	<5.44	CLEO[18]
		2435.9±0.9±5	< 4.6	ARGUS[22]

with respect to the beam direction, the transverse momentum of the muon with respect to the π^0 direction, the impact parameter of the muon at the primary vertex, and finally the reconstructed energy of the D divided by the pion energy.

It would be premature to make a prediction of how many events we might observe, but it is likely that we will produce on order 10,000 $D^+ \rightarrow \mu\nu_\mu$ decays.

1.1.4 D** Spectroscopy

Here the effort would be to study and identify all D** (P wave)states and to categorize the states. As the total spin can be 0 or 1, this leads to the possible states $^3P_2$,$^3P_1$,$^1P_1$, and $^3P_0$. The parities of the states are all positive oweing to the odd angular momentum. The decays one studies are $D^*\pi$ and $D\pi$.

The D_s^{**} states will also be interesting and will be investigated. At the present time the D** spectroscopy needs new data. The World data is presented in Table 4.

The Particle Data Group(PDG) reports that the spin and parity of all these states need confirmation. The states at a mass of 2440 MeV/c^2 and 2470 MeV/c^2 have been omitted from the PDG summary table as too weak. Much more work is needed in pinning down the L=1 charm states. With one order of magnitude more data, this experiment should significant contributions.

1.1.5 Baryon Spectroscopy and Lifetimes

The observation of charmed baryons requires large statistics and good particle identification. In addition the experiment must have excellent ability to reconstruct hyperons. The proposed experiment will be unique in its abilites to study charmed baryon spectroscopy and decay.

At present, E687 has reconstructed many different decay channels of the Λ_c^+. Some of these channels are displayed in figures 3-5. Charmed meson decays

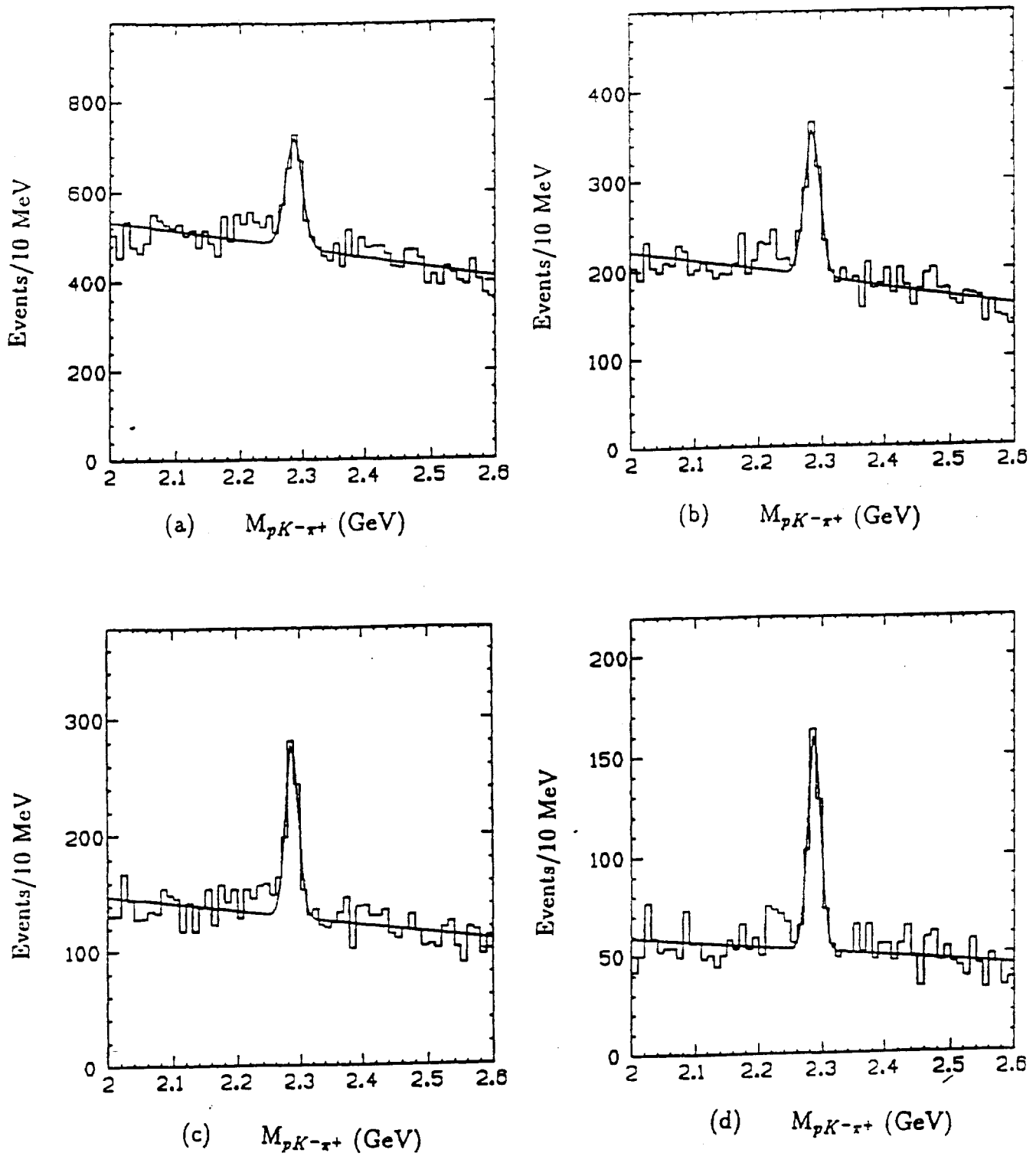

Figure 3: $pK^-\pi^+$ + charge conjugate invariant mass plots showing reconstructed Λ_c^+'s for different vertexing cuts. (a) L/σ_L >4 (no other vertexing cuts), 927±72 fitted events (b) L/σ_L >6 (no other vertexing cuts), 665±53 fitted events (c) L/σ_L >4 and isolation cuts, 424±36 fitted events (d) L/σ_L >6 and isolation cuts, 344±28 fitted events.

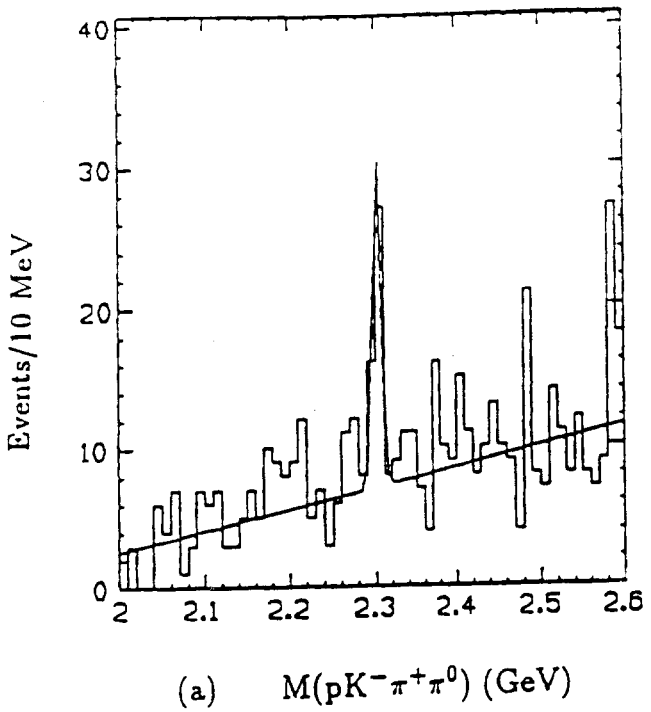

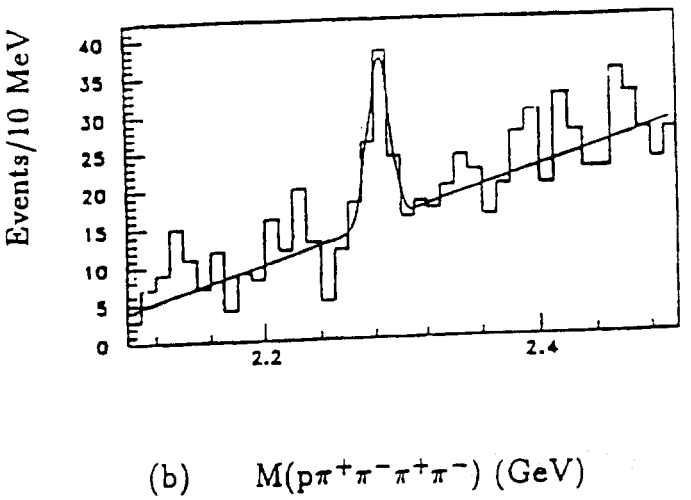

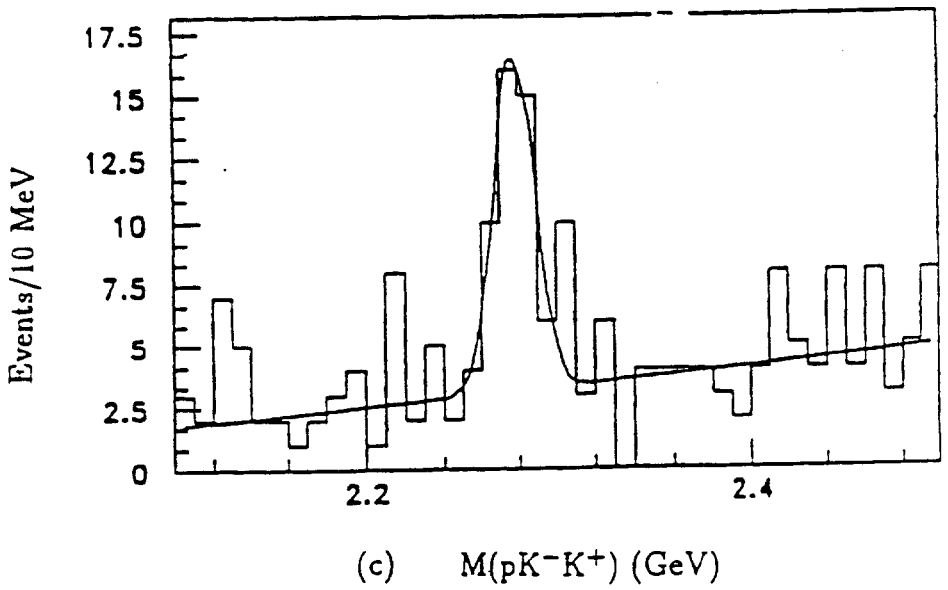

Figure 4: (a) $pK^-\pi^+\pi^0$ + c.c. invariant mass showing reconstructed Λ_c^+'s, the π^0's were reconstructed in the Inner Electromagnetic Calorimeter and the two photon invariant mass was requirede to be within ± 35 MeV of the π^0 mass. (b) $p\pi^+\pi^+\pi^-\pi^-$ + c.c. invariant mass showing reconstructed Λ_c^+'s (c) pK^-K^+ + c.c. invariant mass.

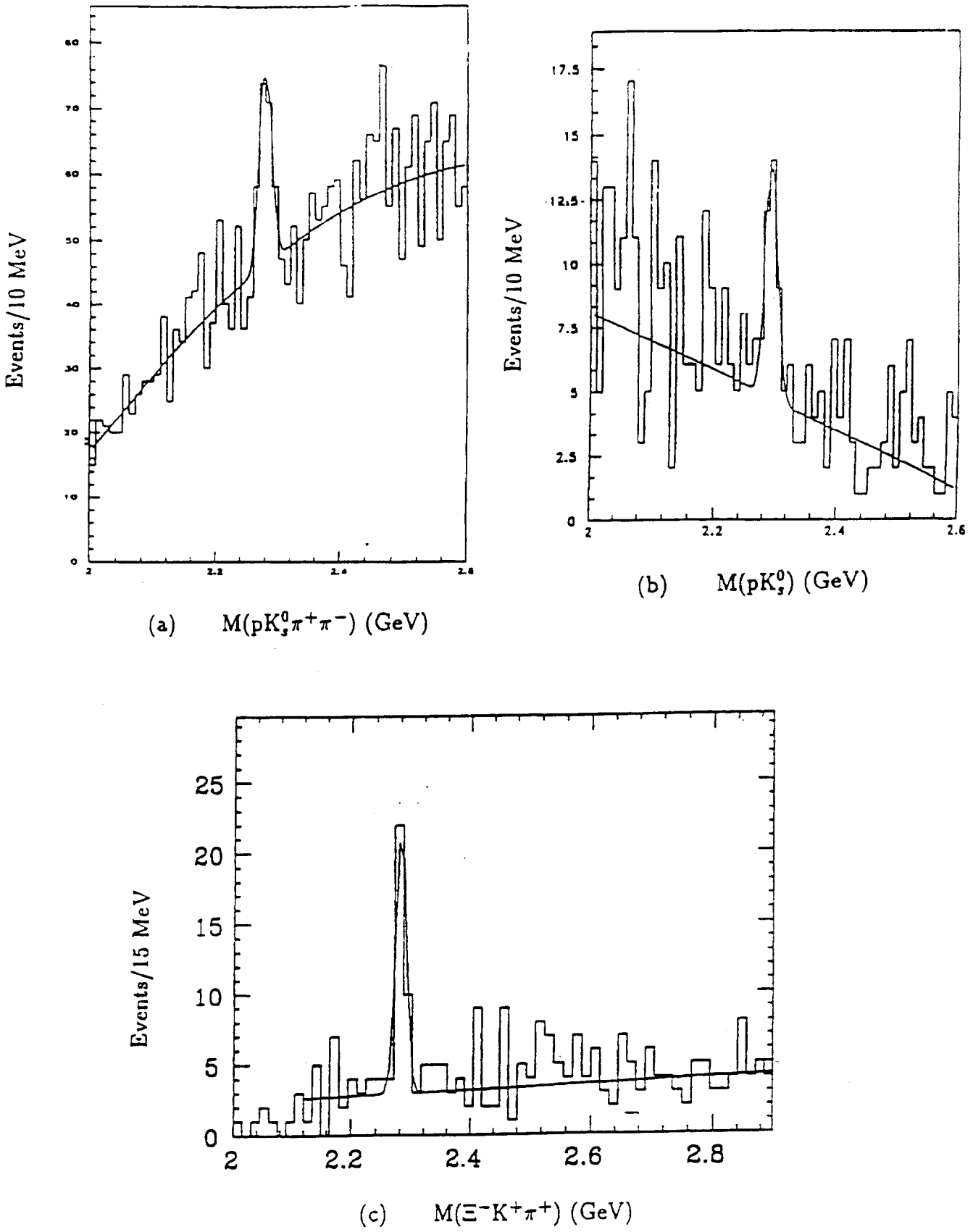

Figure 5: (a) pK$^0_s\pi^+\pi^-$ + c.c invariant mass showing reconstructed Λ_c^+'s. (b) pK^0_s + c.c. invariant mass (c) Ξ^-K$^+\pi^+$ + c.c. invariant mass.

Table 5: Predicted yields of charmed baryons

State	Decay	Estimated Events
Λ_c(cud)	p-k-π	10,000
Σ_c(cuu)	add π^+	150
Σ_c(cdd)	add π^-	300
Ξ_c(csu)	$\Xi^-\pi^+\pi^+$	1,000
Ξ_c(csd)	$\Xi^-\pi^+$	400
Ω_c(css)	$\Omega^-\pi^+$	200

appear to proceed mostly via two-body decays. From the limited information on charm baryon decays this does not appear to be the case. Scaling from last run where we have reconstructed more than 1000 pKπ Λ_c^+ decays, it is expected that 10,000 Λ_c^+ decays can be obtained from this proposed run and maybe a few hundred p-π $-$ π and p-K-K events. The experiment should also start to examine the semileptonic decays of the Λ_c^+.

Another issue is the relative lifetimes of charmed baryons. The lifetime of the Λ_c^+ is much shorter than the lifetime of charmed mesons. This is presumably due to the fact that the decays proceed principally via the W^+ exchange diagram, since for baryons this diagram is neither helicity nor color suppressed. There are two lifetime predictions[23] that differ on whether the Λ_c^+ lifetime is less than or greater than the Ξ_c and the Ω_c. Reliable estimates for the number of reconstructed events we would obtain for these states are possible because we are already observing the states in E687. Figure 6 shows the Ξ_c^0 mass plot of the invariant mass of $\Xi^-\pi^+$ while Figure 7 displays 3 decay channels of the Ξ_c^+. Lastly Figure 8 presents a mass plot of $\Omega^-\pi^+$ which is consistent with the expected mass of the Ω_c^0. It is surprising that E687 has observed the Ω_c^0, however due to excellent hyperon reconstruction the state is seen without requiring a separation from the primary vertex.

It seems likely that the lifetimes for many of these states will be short enough that our resolution will not be able to accurately ($\pm$ 10%) determine the states lifetime. An order of magnitude more data will allow a much more accurate measurement which will put important constraints on models.

In addition to just measuring lifetimes and masses of these charm baryons the experiment will search for excited baryons which decay hadronically to these ground state baryons. We expect to observe excited charm baryons as well as possible decays of doubly charmed baryons. In table 5 we estimate the predicted yields of charm baryons to be observed in this experiment.

From the table it seems that the experiment will make a major contribution in addressing baryon lifetime questions and in determining the baryon mass spectra.

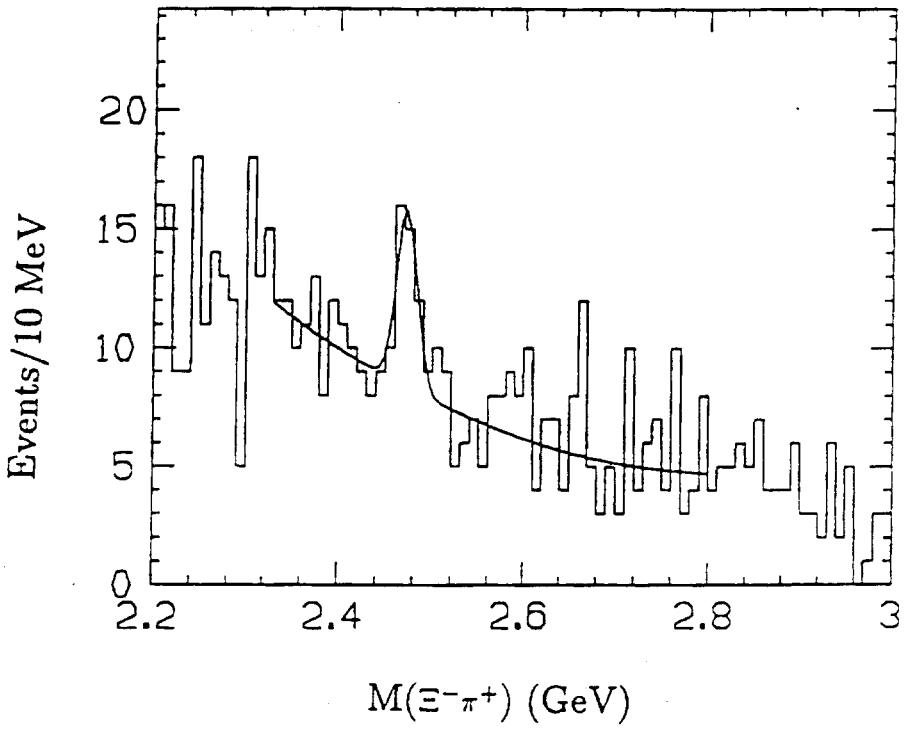

Figure 6: $\Xi^-\pi^+$ + c.c. invariant mass showing reconstructed Ξ_c^0's.

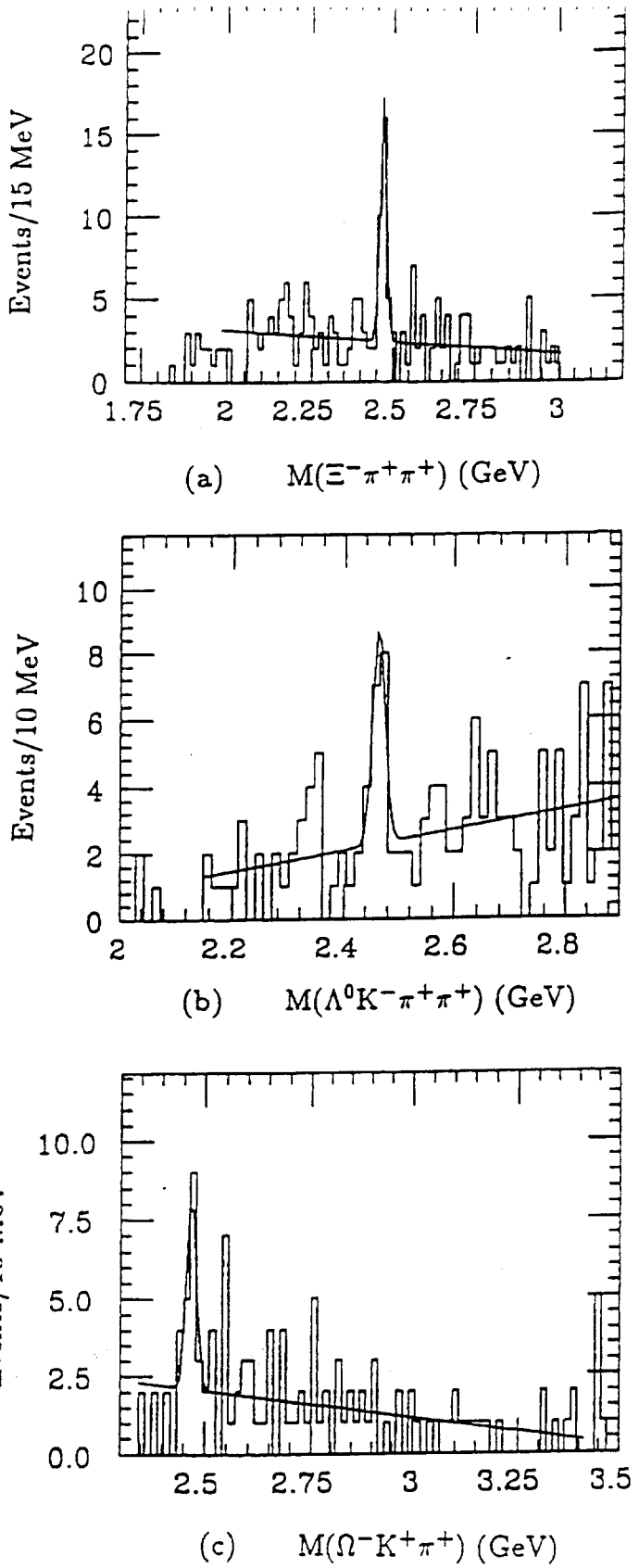

Figure 7: (a) $\Xi^-\pi^+\pi^+$ + c.c. invariant mass showing reconstructed Ξ_c^+'s. (b) $\Lambda^0 K^-\pi^+\pi^+$ + c.c. invariant mass showing reconstructed Ξ_c^+'s. (c) $\Omega^- K^+\pi^+$ + c.c. invariant mass showing reconstructed Ξ_c^+'s.

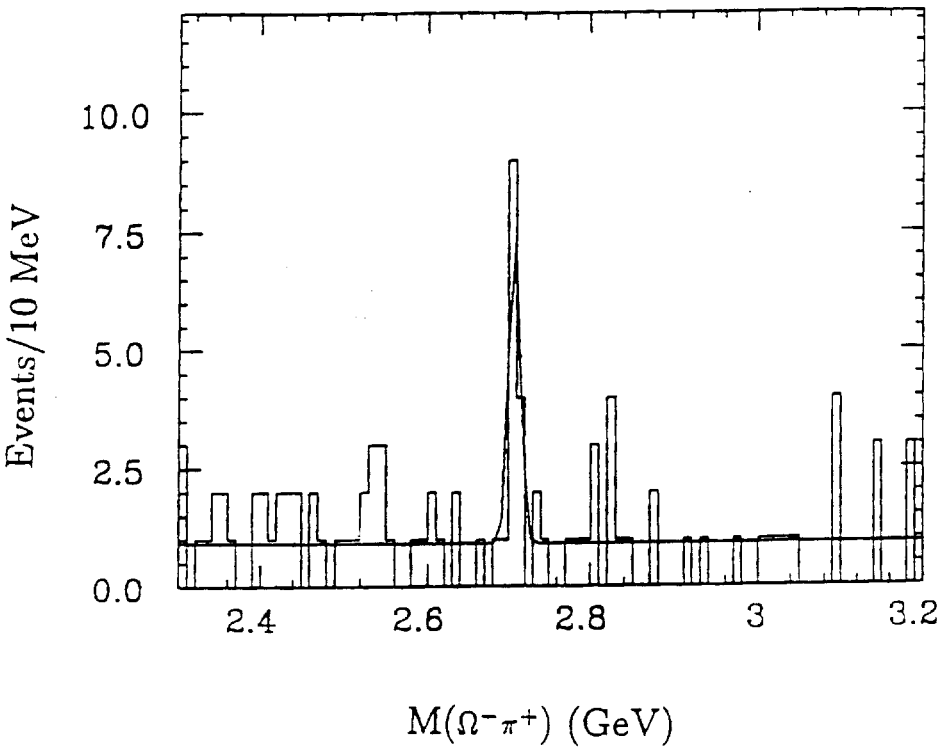

Figure 8: $\Omega^-\pi^+$ + c.c invariant mass showing reconstructed Ω_c^0's

1.1.6 Charm Photoproduction Dynamics

Although this experiment emphasizes the study of charm decay processes, there is a great deal of interesting charm photoproduction physics which we can address with our anticipated yield of 1 million fully reconstructed charm events. We are particularly excited about the possibilities of making detailed studies of charm photoproduction using events with 2 fully reconstructed charm particles. The physics emphasis of such studies would include:

- Tests of charm particle species correlations. For example, how often are baryon-antibaryon pairs produced? Are D_s^+ mesons made with associated D^0 mesons and kaons or are they usually made as D_s - $\bar{D}_s$ pairs? What additional particles are created at the charm primary vertex?

- Tests of Charm dressing and gluon radiation phenomena. In the absence of dressing and/or gluon radiation effects photoproduced charm mesons will carry essentially all of the photon lab energy and will be fully acoplanar (back to back transversely) with the incident photon. Measurements of the charm-$\overline{\text{charm}}$ acoplanarity and fraction of the incident photon energy carried by charm-$\overline{\text{charm}}$ pair serves as a direct measurement of dressing and gluon radiation effects which can be compared to theory and standard Monte Carlo simulations such as LUND. The theoretical acoplanarity distribution due to multigluon radiation has been computed[26] for the case of charm hadroproduction.

- Tests of the validity of the photon gluon fusion model. A powerful test of this model involves measurement of the angular distribution between the charm particle and the photon in the charm-$\overline{\text{charm}}$ center of mass. This distribution is expected to become more forward-backward peaked with increasing charm-$\overline{\text{charm}}$ mass as t and u channel poles of the underlying partonic matrix element approach realization.

- Measurement of the gluon structure function of the nucleon. In the photon-gluon fusion model, the cross section for charm photoproduction is directly proportional to the gluon structure function $g(x)$ rather than a convolution over two structure functions as is the case in hadroproduction. The gluon structure of the nucleon controls x distribution of charm event where x is square of charm-$\overline{\text{charm}}$ mass divided by the overall center-of-mass energy. We anticipate making direct measurements of $g(x)$ over the range $0.03 < x < 0.25$.

Using about 1/2 of the E687 data set, we have recently[27] obtained a very clean sample of 200 events with two fully reconstructed D's decaying into the final states $D^o \rightarrow K^-\pi^+$, $K^-\pi^+\pi^+\pi^-$ and $D^+ \rightarrow K^-\pi^+\pi^+$ final states. This sample is about an order of magnitude larger than previous published of fully reconstructed, photoproduced $D\overline{D}$ events[28] In the next experiment we

anticipate a 5000 event sample. The $D\overline{D}$ signal and some of its properties which bear on charm production dynamics are illustrated in Figure 9. This signal has been augmented with a 2000 event sample obtained from 1/2 of the E687 data set where a fully reconstructed D was found recoiling against a kinematically isolated π from the process $D^o \rightarrow \pi D$. This sample allows one to perform many of the same production dynamics studies as the fully reconstructed $D\overline{D}$ sample since the kinematically isolated π's momentum can be suitably scaled up to provide an accurate estimate of its parent D^{*+} momenta.

1.2 High Impact Physics

1.2.1 Absolute Branching Ratios

We believe that it will be possible to obtain competitive measurements of absolute charm branching ratios in this experiment using the decay $D^{*+} \rightarrow \tilde{\pi}^+ D^o$ where presence of a photoproduced D^o can be inferred by kinematically tagging the decay pion (which we will call the $\tilde{\pi}$). The fraction of times that a $\tilde{\pi}$ tagged D^o is observed to decay into a given final state serves to measure its absolute branching ratio.

The $D^{*+} \rightarrow \pi^+ D^o$ tagging technique exploits a P_t and charge-charm correlation between the D^{*+} decay pion and the recoiling, anti-charmed particle. Because of the low Q value for the process $D^{*+} \rightarrow \pi^+ D^o$, the decay pion will have a lab momentum nearly collinear with the parent D^{*+} but diminished by roughly the ratio of the pion mass over the mass of the D^{*+} or a factor of about 1/13.8[24]. Because the P_t's of photoproduced charmed and anticharmed particles are expected and observed[25] to balance to within few GeV, one expects that true $\tilde{\pi}$'s should cluster at small values of

$$\Delta_x = 13.8 P_x^{(\tilde{\pi})} + P_x^{(r)} \quad \text{and} \quad \Delta_y = 13.8 P_y^{(\tilde{\pi})} + P_y^{(r)}$$

relative to the $\vec{P}^{(r)}$ momentum carried by the observed, recoil anti-charmed particle.

We have searched for the expected $\tilde{\pi}$ correlation in our 1990 data where we have use a large, clean sample of reconstructed recoil charm candidates (See Fig. 10) decaying via: $D^o \rightarrow K^-\pi^+$ & $K^-\pi^+\pi^-\pi^+$ and $D^+ \rightarrow K^-\pi^+\pi^+$. Because of their ease of reconstruction, low background contamination, and relatively large branching ratio's, we will call these *golden* mode charm decays.

We look for $\tilde{\pi}$ events among those tracks which are in the primary vertex[29] for the events with a reconstructed charm particle. The recoil charm particle must lie within 2σ of its nominal mass. Equal width (normalized) mass sidebands are used to subtract recoil charm background. Figure 10 is shows Δ_x distribution for those primary vertex tracks subjected to the cut $\Delta_y < 1$ GeV. The points joined by the upper solid curve correspond to "right sign" tracks which have an electrical charge equal and opposite to the charm of the recoil charm particle. The point joined by the dashed curve correspond to "wrong

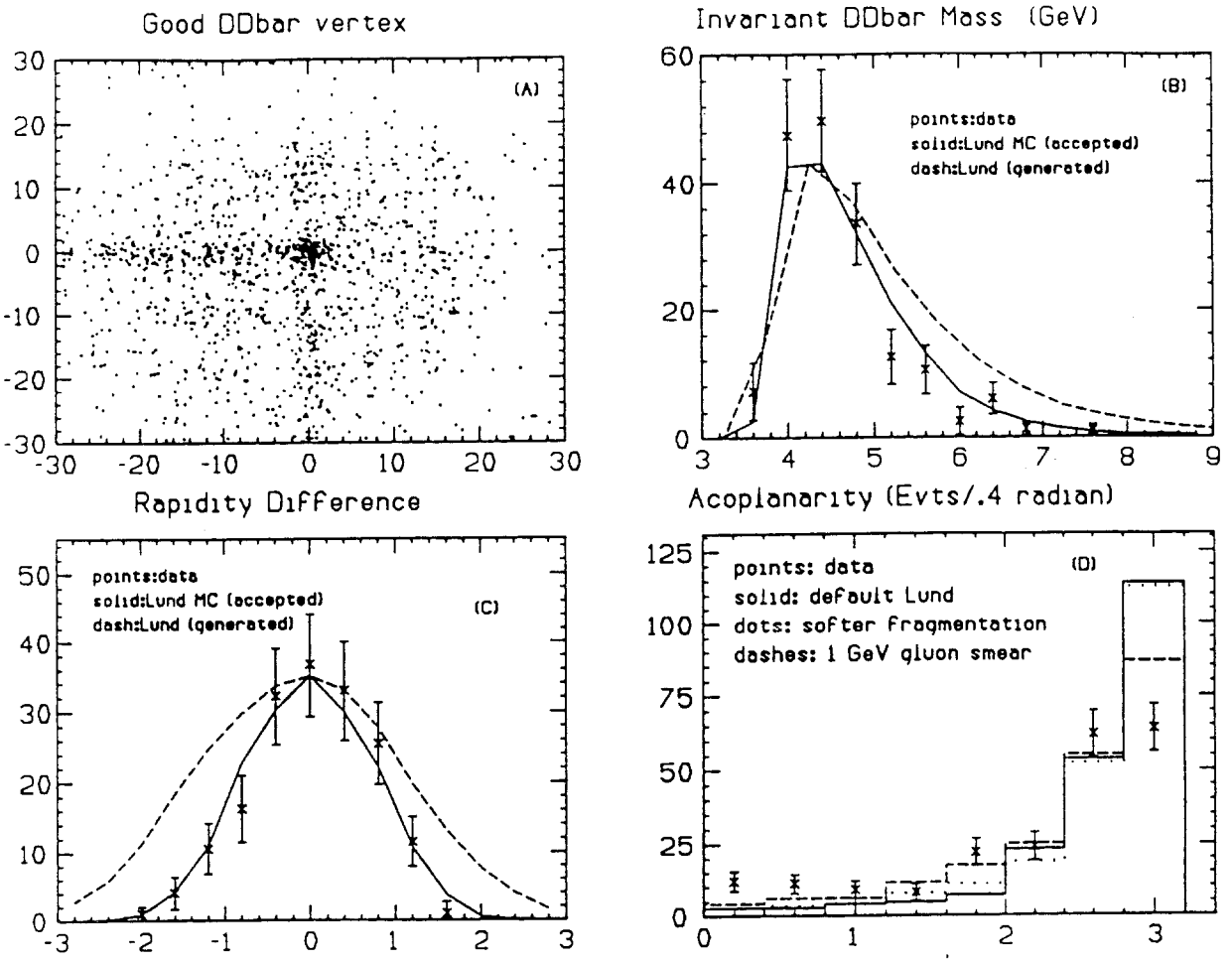

Figure 9: (a) Scatter plot of the normalized mass of detached D candidate versus the normalized mass of the detached, recoil $\overline{D}$ candidate where the recoil D is required to intersect the plotted D with an acceptable vertex confidence level. (b) The background subtracted invariant mass of the $D\overline{D}$ pair compared to the Monte Carlo (solid curve). (c) Rapidity difference ($Y_D - Y_{\overline{D}}$) distribution between the reconstructed D and $\overline{D}$. The distribution is background subtracted and compared to the solid curve computed using the Monte Carlo. (The dashed curves in figures (b-c) represent generated distributions without acceptance effects.) (d) Background subtracted acoplanarity distribution compared to the Monte Carlo (solid curve). The acoplanarity (in radians) is the angle between the plane containing the D momentum and the incident photon and the plane containing the $\overline{D}$ momentum and the incident photon. Several different choices of Monte Carlo parameters are compared.

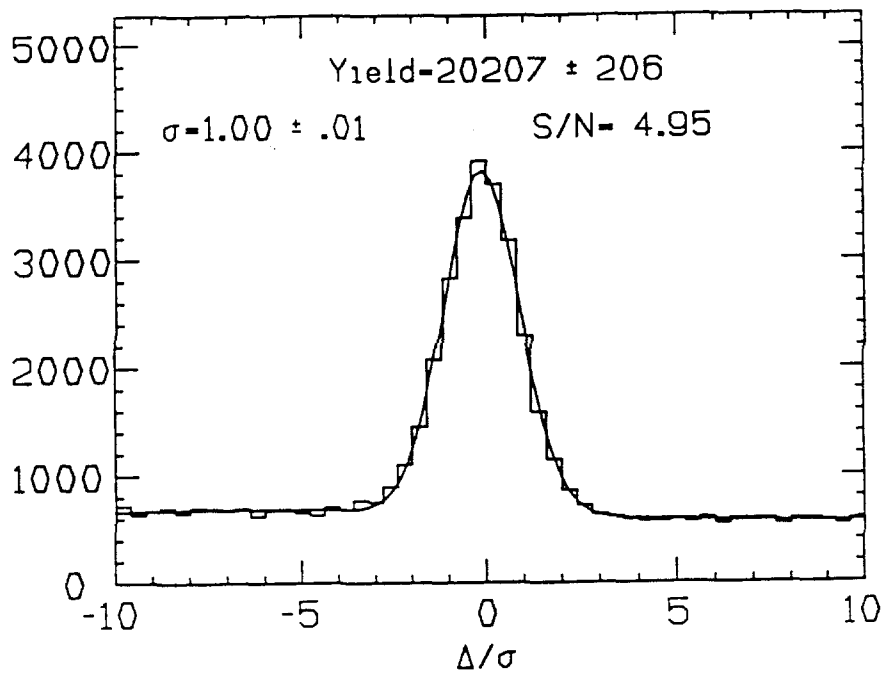

Figure 10: Normalized mass distributions(in measurement standard deviations away from nominal value, $\Delta M/\sigma$) for $D^+ \rightarrow K^-\pi^+\pi^+$, $D^0 \rightarrow K^-\pi^+$, $D^0 \rightarrow K^-\pi^+\pi^+\pi^-$, candidates obtained in the 1990 run of E687 subject to topology dependent vertex detachment cuts ranging from 1 to 10 standard deviations as well as vertex isolation cuts. A signal of 20000 events is observed with a signal to noise of about 5 to 1 and a Gaussian RMS normalized width consistent with unity

sign" tracks. A clear excess of right sign over wrong sign tracks is observed at $\Delta_x \approx 0$.

Figure 11 compares subtracted distributions of the variable $\Delta_t^2 \equiv \Delta_x^2 + \Delta_y^2$ for tracks in the primary vertex against a recoil charm particle. The upper points are right sign tracks, the lower points are wrong sign tracks. The two curves (right sign solid, wrong sign dashed) are simulated LUND - Pythia - Jetset Monte Carlo[27] Δ_t^2 distributions normalized to the same number number of inclusive D's shown in Figure 10. There is reasonable agreement between the absolutely normalized Monte Carlo and data in both the anticipated level and shape of the wrong sign $\tilde{\pi}$ background. The Δ_t^2 distribution for right sign $\tilde{\pi}$ tracks is somewhat broader in data than in Monte Carlo. This effect is also observed in Figure 12 for the $|\vec{P}_t|$ distribution in fully reconstructed D- $\overline{D}$ events. Presumably the real world has somewhat more severe dressing effects than those simulated in Monte Carlo.

The general agreement between data and Monte Carlo helps bolster the case that the $\tilde{\pi}$ events are indeed tags for D^{*+} and can be used to provide absolute neutral D branching ratios.

Since the $\tilde{\pi}$ sample is observed to be 10 % of the inclusive D sample, P831 should produce a huge ($\approx$ 50000 event) $\tilde{\pi}$ sample which can be used to study tagging systematics and backgrounds. The primary source of error on absolute branching ratio measurement using the soft pion technique will be statistical. The soft pion technique requires that both the charm and anti-charm particle in a given event are fully reconstructed. The reduced acceptance from requiring 2 D's and additional branching ratios will result in a considerably smaller expected D - $\overline{D}$ sample than that for either the $\tilde{\pi}$ or inclusive golden mode D sample. Because, the relative branching ratio of the different D^o golden modes will be measured to high statistical precision from the very copious inclusive sample, the fractional error common to each absolute branching ratio will be the fractional error on the total number of golden mode D $\overline{D}$ events of events of the form: $\overline{D}D^{*+} \rightarrow \overline{D}(\pi^+ D^o)$. We can estimate this number using our experience with E687.

In the 1990 data of E687, we observed a yield of 200 reconstructed $D - \overline{D}$ events into the three golden decay modes $K^-\pi^+\pi^+$, $K^-\pi^+$ and $K^-\pi^+\pi^+\pi^-$. Scaling up by the anticipated luminosity for P831 we expect a 5000 event sample with both a reconstructed golden mode D and $\overline{D}$. About 62 % of these events will have a clean golden mode D^o recoiling against a golden mode D^o or D^+. About 20 % of the events with a golden mode D^o will actually originate from $D^{*+} \rightarrow \pi^+ D^o$ decay[30] with an accepted, reconstructible π^+. Hence about 620 events or 13 % of the 5000 event total D - $\overline{D}$ golden mode sample is usable for purposes of measuring absolute neutral D branching ratios which implies a 4 % fractional error on absolute D branching ratios where only the three golden modes are considered.

The inclusion of additional decay modes will of course further reduce the fractional error below the projected 4 % estimate from P831 using just the golden

831

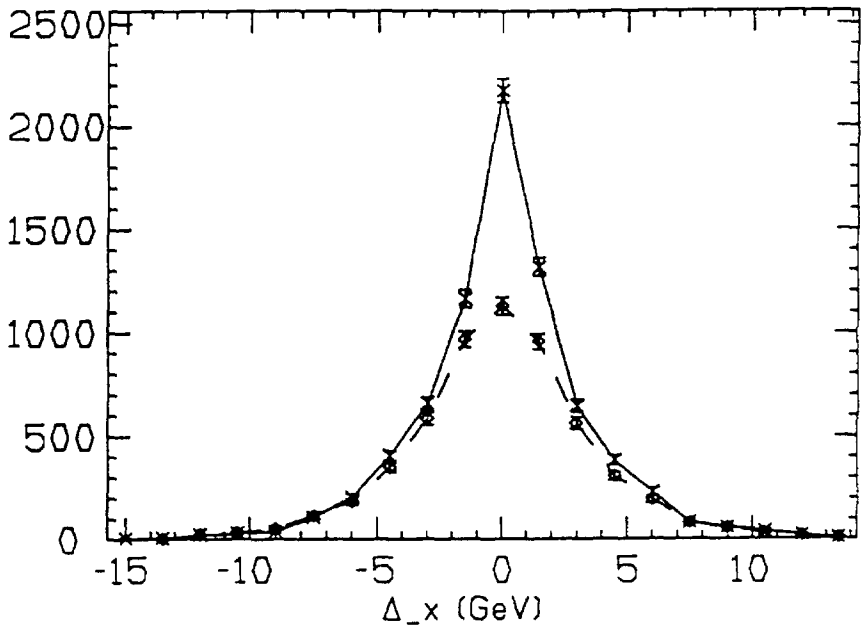

Figure 11: Background subtracted Δ_x distribution for primary vertex tracks satisfying the cut $\Delta_x < 1$ GeV. The upper solid curve is for (right sign) tracks with a charge not equal to the recoil charm; the lower dashed curve is for (wrong sign) tracks. A clear excess of right sign over wrong sign tracks is observed at Δ_x , $\Delta_y \approx 0$ indicating a strong signal for the $\bar{\pi}$

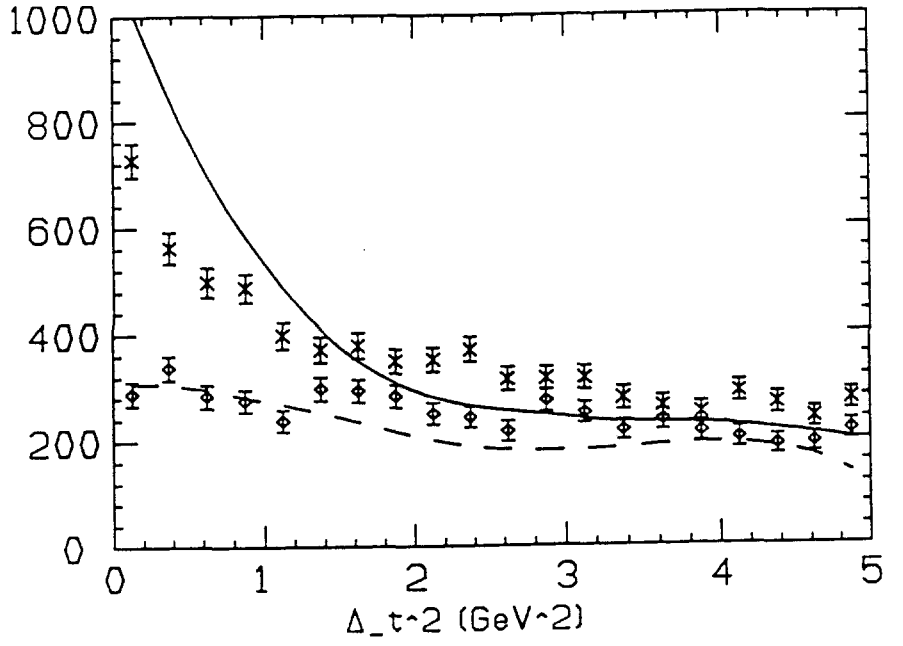

Figure 12: Background subtracted Δ_t^2 distribution for primary vertex tracks. The upper curve (x's) are for right sign tracks. The lower curve (diamonds) are for wrong sign tracks. The upper solid curve is from an absolutely normalized Monte Carlo for right sign tracks; the lower curve is an absolutely normalized Monte Carlo for wrong sign tracks. The Monte Carlo predicts a softer P_t^2 distribution than the data for $\tilde{\pi}$ events but the level of signal and background and background shape is well predicted.

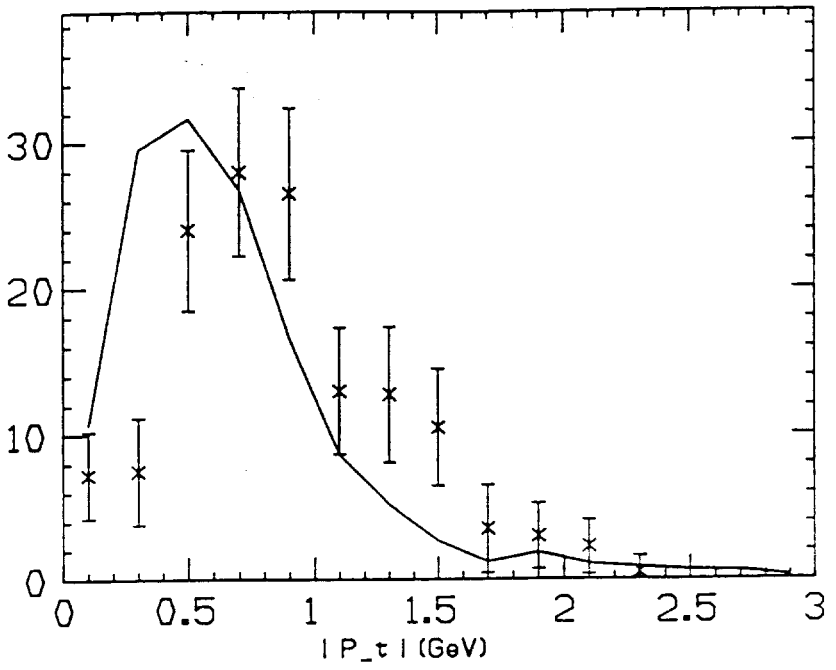

Figure 13 Distribution for $|\bar{P}_t|$ where $\bar{P}_t$ is vector sum of the transverse momenta carried by the D and $\overline{D}$ events in events where both D and $\overline{D}$ are reconstructed into the final states $K\pi$, $K2\pi$, or $K3\pi$. The data is background subtracted using D and $\overline{D}$ mass sidebands. The solid curve is a LUND Monte Carlo simulation.

modes. We estimate that as much as a factor of two reduction in this fractional error will be possible through the use of additional charm decay modes. Baryon and D_s^+ decays can be used along with golden and non-golden D decays to increase the number of $\bar{\pi}$ tags. The absolute branching for additional, non-golden D^o decays can be included in a global fit (using well measured branching ratios relative to the golden modes) to improve the absolute branching ratio measurement for all neutral D modes. Since the $\bar{\pi}$ tagging method requires the presence of a D^*, a particularly useful class of additional neutral D's are decays into final states with a single missing neutral particle which can be reconstructed exploiting the favorable kinematics of $D^* \rightarrow D^o\pi^+$ decay. Examples include $D^o \rightarrow K^-\pi^+\pi^o$ (with roughly $3\times$ the $K^-\pi^+$ branching ratio) and $D^o \rightarrow K^-\ell^+\nu$ (with a branching roughly equal to that of $K^-\pi^+$ for both the μ^+ and e^+ decay). Very clean $D^* - D$ mass difference peak signals can be obtained[31] for these decay modes by using the D flight direction (measured by the line between the primary and secondary vertex) and the D mass constraint to correct for the momentum of the missing neutral.

Using the 1990 data sample of E687, we have demonstrated that it is possible to tag neutral D's by tagging the pion from $D^{*+} \rightarrow D^o\pi^+$ decays. We have also obtained a sample of about 200 fully reconstructed D, $\overline{D}$ decays into the three golden modes: $K^-\pi^+$ & $K^-\pi^+\pi^-\pi^+$&$K^-\pi^+\pi^+$. Scaling up our previous results by the anticipated luminosity of P831, we should obtain a fractional error on absolute charm branching ratios of 4 %. We believe that it will be possible to improve this fractional error as much as an additional factor of 2 by considering additional charm species and charm decay modes. We expect to produce a new measurement with complementary systematics which is highly competitive with the existing measurements of charm absolute branching ratios. The present numbers are dominated by recent measurements from ALEPH and older measurements from MarkIII which each have fractional errors on absolute charm branching ratios in the range 12-15%.

1.2.2 CP Violation

It has been shown [33] that CP violations in the decay of charm mesons may be significantly enhanced over naive expectactions, without requiring new physics in addition to the standard model. The enhancement is due to strong interactions. The signature for CP violation would be an asymmetry in the decay rate of a Cabibbo suppressed mode and its CP conjugate:

$$\Gamma(D \rightarrow f_{CS}) \neq \Gamma(\overline{D} \rightarrow \bar{f}_{CS}) \tag{6}$$

Cabibbo suppressed modes are required because, in order to exhibit a CP asymmetry, there must be two independent amplitudes that contribute to the same final state. In addition, final state interactions must induce a strong phase shift between the two amplitudes [32] Charm decays are therefore ideal, since they exhibit significant final state interactions. CP violating asymmetries of a few

percent are possible in the standard model [33]. If new physics is introduced into the standard model (extra Higgs multiplets, for example), then asymmetries as large as 10% are possible [32]. This experiment will be sensitive to asymmetries of a few percent in at least two decay modes, and will be sensitive to a 10% asymmetry in at least three modes. In this section, we will first discuss in detail a search for such a decay rate asymmetry, then briefly mention two additional CP violation search strategies.

We will use the following three "high statistics" Cabibbo suppressed decay modes (and their charge conjugates) to search for a CP induced decay rate asymmetry:

$$\begin{aligned} D^+ &\to & K^+K^-\pi^+ \text{ (i)} \\ D^{*+} &\to \pi^+ D^0; & D^0 &\to K^+K^- \text{ (ii)} \\ D^{*+} &\to \pi^+ D^0; & D^0 &\to \pi^+\pi^- \text{ (iii)} \end{aligned} \tag{7}$$

In reactions (ii) and (iii), the sign of the bachelor pion in the D^* decay tags the neutral D as either a D^0 or a $\overline{D}^0$. We will refer to these as "D^*-tagged" D^0 decays.

Consider for the moment reaction (i). If equal numbers of D^+ and D^- mesons are produced, then the CP decay rate asymmetry is:

$$\begin{aligned} A_{CP}(KK\pi) &\equiv \frac{\Gamma(D^+\to K^+K^-\pi^+)-\Gamma(D^-\to K^+K^-\pi^-)}{\Gamma(D^+\to K^+K^-\pi^+)+\Gamma(D^-\to K^+K^-\pi^-)} \\ &= \frac{N(D^+\to K^+K^-\pi^+)-N(D^-\to K^+K^-\pi^-)}{N(D^+\to K^+K^-\pi^+)+N(D^-\to K^+K^-\pi^-)} \end{aligned} \tag{8}$$

where $N(D^+ \to K^+K^-\pi^+)$ is the number of reconstructed decays, measured by fitting the mass plot of appropriately selected $K^+K^-\pi^+$ combinations. Similar asymmetry parameters, $A_{CP}(KK)$ and $A_{CP}(\pi\pi)$, can be defined for reactions (ii) and (iii).

It is not necessary to assume equal production, however. The relative D^+/D^- and D^{*+}/D^{*-} production rates can be determined using the Cabibbo favored decay modes:

$$\begin{aligned} D^+ &\to & K^-\pi^+\pi^+ \text{ (iv)} \\ D^{*+} &\to \pi^+ D^0; & D^0 &\to K^-\pi^+ \text{ (v)} \\ D^{*+} &\to \pi^+ D^0; & D^0 &\to K^-\pi^+\pi^-\pi^+ \text{ (vi)} \end{aligned} \tag{9}$$

and their charge conjugates. These decay modes will not exhibit a CP induced rate asymmetry in the standard model. Since these decays are each roughly an order of magnitude more plentiful than the Cabibbo suppressed modes above, their contribution to the uncertainty in A_{CP} will be small. Using reaction (iv) to correct (i) for the measured D^+/D^- production rates, one obtains:

$$A_{CP}(KK\pi) = \frac{\eta(D^+ \to K^+K^-\pi^+) - \eta(D^- \to K^+K^-\pi^-)}{\eta(D^+ \to K^+K^-\pi^+) + \eta(D^- \to K^+K^-\pi^-)} \tag{10}$$

Table 6: Projected Asymmetry Measurement

Decay Mode	# Reconstructed	$\sigma(A_{CP})$	90% CL Upper Limit
$KK\pi$	15000	1.7%	2.8%
KK	5000	2.9%	4.8%
$\pi\pi$	1500	5.2%	8.6%

where

$$\eta(D^+ \to K^+K^-\pi^+) = \frac{N(D^+ \to K^+K^-\pi^+)}{N(D^+ \to K^-\pi^+\pi^+)}$$

A similar change for the D^*-tagged modes is necessary, where

$$\eta(D^0 \to P^+P^-) = \frac{N(D^0 \to P^+P^-)}{N(D^0 \to K^-\pi^+) + N(D^0 \to K^-\pi^+\pi^-\pi^+)}$$

and $P^+P^- = K^+K^-, \pi^+\pi^-$.

Assuming we achieve our goal of 10^6 reconstructed charm decays, we will observe approximately $100,000$ D^*-tagged $D^0/\overline{D}^0 \to K^\mp\pi^\pm, K^\mp\pi^\pm\pi^-\pi^+$ decays, and $250,000$ $D^\pm \to K^\mp\pi^\pm\pi^\pm$ decays. Table 6 shows the number of reconstructed $KK\pi$ and D^*-tagged KK, $\pi\pi$ events we would expect. The table also shows the resulting error in the asymmetry measurement, and the 90% confidence level upper limit we would set on $|A_{CP}|$ for each mode if we saw no effect. We have included in our error calculation the assumption that the mass plots used to fit for the number of events in each decay have a signal to noise of about 1:1. Our estimates for the number of events we will reconstruct are all scaled from signals already observed by E687, with the exception of the $\pi\pi$ decay mode. Note that the strong phase shift due to final state interactions will most likely be different for the three modes, so that each mode is not necessarily expected to exhibit the same asymmetry.

The systematic errors in this measurement should be negligible. For the D^*-tagged modes, systematics would have to be due to a charge dependent efficiency for finding the bachelor pion. A similar systematic error would also be necessary for the D^+ decay modes. Such a systematic error should be very small, and in any case it would have to be present for the Cabibbo suppressed modes, but not for the Cabibbo favored modes, which seems unlikely.

There are two additional methods [32] we will use to search for evidence of CP violation in charm decay. The first is to look for a time dependent asymmetry in decay modes (ii) and (iii), induced by $D^0 - \overline{D}^0$ mixing. A search for such an asymmetry is very similar to a search for mixing. An observable asymmetry requires the existence of both mixing and a CP violating difference in the decay amplitudes. The second method involves looking for CP asymmetries in final state correlations of the decays of charm mesons to two vector particles, such

Table 7: Limits on Rare D Decays

Decay Mode	Type of Test	Limit on 90% CL	Experiment
$D^+ \to \pi^+ e^+ e^-$	FC	$< 2.5\times 10^{-3}$	Mark2
$D^+ \to \pi^+ \mu^+ \mu^-$	FC	$< 2.9\times 10^{-3}$	CLEO
$D^+ \to \pi^+ e^\pm e^\mp$	LF	$< 3.8\times 10^{-3}$	CLEO
$D^+ \to K^+ e^+ e^-$		$< 4.8\times 10^{-3}$	Mark2
$D^+ \to K^+ \mu^+ \mu^-$		$< 9.2\times 10^{-3}$	Mark2
$D^+ \to \pi^- e^+ e^+$	L	$< 4.8\times 10^{-3}$	Mark2
$D^+ \to \pi^- \mu^+ \mu^+$	L	$< 6.8\times 10^{-3}$	Mark2
$D^+ \to \pi^- e^+ \mu^+$	L	$< 3.7\times 10^{-3}$	Mark2
$D^+ \to K^- e^+ e^+$	L	$< 9.1\times 10^{-3}$	Mark2
$D^0 \to e^+ e^-$	FC	$< 1.3\times 10^{-4}$	MKIII
$D^0 \to \mu^+ \mu^-$	FC	$< 1.1\times 10^{-5}$	E615
$D^0 \to \mu^\pm e^\mp$	LF	$< 4.1\times 10^{-5}$	E691
$D^0 \to K^0 e^+ e^-$	FC	$< 1.7\times 10^{-3}$	MKIII
$D^0 \to \rho e^+ e^-$	FC	$< 4.5\times 10^{-4}$	CLEO
$D^0 \to \rho \mu^+ \mu^-$	FC	$< 8.1\times 10^{-4}$	CLEO

as $D^+ \to \overline{K}^{*0} K^{*+}$. For example, one could investigate the triple correlation:

$$C_+ = \left\langle \overrightarrow{p_0} \cdot \left(\overrightarrow{\epsilon_0} \times \overrightarrow{\epsilon_+} \right) \right\rangle .$$

CP violation would manifest itself as a non-zero sum of C_+ and C_- (C_- is the triple correlation for the CP conjugate decay).

1.2.3 Rare and Forbidden Leptonic Decays

These decays have sensitivity to new kinds of physics. While it is very difficult to compete with the severe upper limits which have been set by Kaon decays, there are superstring[34], lepto-quarks[35], and technicolor[36] models in which large flavor-changing neutral current effects would be present in charm decays, but not in kaon decays.

The searches in this experiment should significantly lower the limits of charm decays to leptons in two and three body decays.

In table 7 a list of limits are tabulated. A more complete listing of limits and references can be be found the the latest PDG particle summary book. Following the PDG group we refer to flavor changing neutral current as (FC), lepton number violation as (L), and lepton family number violating as (LF).

2 Options for Obtaining Higher Flux

We can increase the number of reconstructed charm events by improving the efficiency and acceptance of the spectrometer and by speeding up the data acquisition system (to decrease deadtime). However, the spectrometer already has a rather large acceptance and good efficiency. One can imagine upgrades that will yield a factor of two gain. At least a factor of 5 gain must, therefore, come from increased luminosity. There are several approaches to achieving higher photon intensity. After a brief summary of the beam performance to date, we discuss some of the options.

2.1 Performance of the Wideband Beam

The Wideband beam underwent two upgrades for the 1990-1991 run. The first, the replacement of the beryllium production target by a liquid deuterium target, resulted in an increase in flux by a factor of 1.5, close to the 1.65 that was expected; the second, the use of the positron flux to create photons, resulted in an increase in flux of about 1.5. However, the positron beam had much more "hadronic background" than we expected and was never fully utilized. We investigated this hadronic background from two directions. One effort involved developing a trigger that rejected the hadronic background on the positive side. By the end of the run, the effort had almost produced a successful trigger and offline work has now produced a trigger strategy that will work. The second effort tried to identify and eliminate the hadronic background. It is now rather convincingly established that the background is from Λ decays between the downstream end of the target box sweeping magnets and the first bend in the beam. In the 1991 run roughly one-half of the hadronic background was eliminated by adding a dipole magnet between the downstream end of the target box and the first quadrupole. We believe that with our present understanding we can use the positron beam for real data-taking in the future. The yield in the electron beam at 350 GeV/c is 4.8×10^{-5} electrons per incident 800 Gev/c proton. If the positron beam is used this becomes 7.0×10^{-5} electrons per incident 800 GeV/c proton.

2.2 Options for Increasing the Flux

2.2.1 Change in Incident Beam Energy

If Fermilab is able to upgrade the proton beam energy, the electron beam flux will increase accordingly. A primary proton energy increase from 800 to 900 GeV/c will result in an improvement of about 1.86 in the secondary electron flux at the nominal momentum setting of 350 GeV/c. The electron flux increase will be a factor of 1.68 if the secondary momentum is set for a mean value of 250 GeV/c.

2.2.2 Change in Secondary Beam Momentum

By emphasizing charm physics, it is possible to improve the charm yield by dropping the secondary beam momentum. If the mean momentum is lowered to 250 GeV/c from our standard setting of 350 GeV/c, then the flux should increase by a factor of three (and the relative background in the positron beam will drop quite a bit).

During the 1991 fixed target run a test was performed to measure the electron and positron yield at the 250 GeV setting as well as the hadron contamination. The results can be summarized as follows: In normal running at the 350 GeV negative setting, the beam has 8% pion contamination. If the beam is run with a 350 positive setting, then the positron yield is 50% of the electron yield, but the positive hadron contamination is 60% of the beam. At the 250 GeV setting the electron yield is measured to be 2.64 times larger than the 350 GeV setting. The hadron contamination is now only 6%. At a positive 250 GeV setting the hadron contamination is only 26% while the positron yield is again 50% of the electron yield, but 2.60 times larger than the 350 GeV setting.

If the positive and negative beams are run at the same time, then the hadron contamination is 14% and yield is 1.4 times larger. Hence the beam behaves as expected. The hadron contamination is lower at the 250 GeV setting and the electron and positron flux is 2.6 times higher than at the 350 GeV setting.

2.2.3 Fixing the Occlusion in the Positron Arm

The positron arm of the beam should have the same yield as the electron side of the beam. Unfortunately there is an occlusion in the vacuum pipe caused by an offset pipe. The positive arm yield could be doubled by fixing this occlusion. If the a simple solution can be found, then we would like to have it repaired. However, we are not dependent on this repair.

2.2.4 Change in Choice of Experiment Parameters

The experimental target can be increased to 15% (from our existing 10%) of an interaction length. In doing this, we lose resolution and acceptance for the interactions in the upstream segments of the target, as the interactions occur further from the microstrip, but do gain in events. We may not gain the entire 50%, but we expect an increase of at least 30%.

It is also possible to increase the radiator. This will increase the number of high energy photons but will also produce dramatically more low energy photons. The ability to do this will depend on how successfully we upgrade the rate capability of the detectors and improve the trigger. It is hard to imagine gaining more than 20-30% by doing this.

Table 8: Summary of luminosity improvements for a charm experiment

	350 GeV	250 GeV	400 GeV
Positrons	1.50	1.50	1.50
Helium in Target Box	1.1	1.1	1.1
Accelerator Upgrade to 900	1.86	1.68	2.6
Change Energy from 350	1.0	2.6	0.7
More Intensity	1.5	1.5	1.5
Total Gains	4.6	10.8	4.5

2.2.5 Increase in the Number of Incident Protons

We could go from 4×10^{12} to 6×10^{12} protons on target per pulse. This gives us another factor of 1.5. The places where we could have trouble transporting this much beam are in the cryogenic bends and in the LD2 target. The LD2 target is rated at 10^{13} and should be ok. The principal problem is the cryo bends. The bends are supposed to be able to take this rate. The bends have taken rates of over 5×10^{12} for short periods of time so there is no reason to believe that this will be a problem. A major question is whether the laboratory would be able to deliver this many protons to us for the duration of the experiment.

2.2.6 Changes in the Production Target

A minor improvement would be to put helium into the target box and extend it up to the quadrupoles. Adding helium would decrease the probability for photons to convert to pairs in the target box and after the converter reduce the bremsstrahlung of electrons and positrons. Thus increases the flux by 10%. The addition of helium also reduces the hadronic contamination.

2.2.7 Summary of 'Beam Options

Table 8 gives a summary of what should be viewed as "conservative" approaches to increasing the luminosity. Note that in this table we have not included changes to the experiment's operating conditions, such as more target or more radiator, which were also discussed above and can result in additional increases in the luminosity. Note we have also not included any change due to a repaired occlusion in the positive arm.

3 Modifications to the apparatus to handle high rates

The main challenge for the apparatus is to be able to handle the increased rate at all levels. Each element will have to operate at at least five times the instantaneous and average rate which it now sees. Because the intensity in the e^+e^- pair region is 500 times that in the rest of the detector, almost all of the difficulties are in the center of the spectrometer. In this section, we discuss how each detector and its associated front-end electronics needs to be modified to handle the increased rates. The required upgrade of the trigger and data acquisition system is also discussed in this section.

3.1 Trigger Counters

To handle an instantaneous rate increase of a factor of 5, our trigger counters will need to be changed. We presently trigger on TR1·TR2·$(\mathrm{H}\times\mathrm{V})_{2\ body}$, where TR1 is a single scintillation counter situated between the target and the silicon microstrip, TR2 is a single scintillation counter located immediately downstream of the microstrip, and H×V is an array of vertical and horizontal counters placed downstream of the last proportional wire chamber, P4. The symbol 2 *body* refers to the fact that we typically require 2 hits in the H×V array. Counters TR1 and TR2 presently operate at $1\mathrm{M}Hz$. At a rate 5 times higher they would barely work.

We have considered two options for replacements of TR1 and TR2. The first option involves replacing these counters with several smaller counters thereby distributing the rate over several phototubes. This choice would obviously work, but since TR1 sets the timing for the entire experiment, then special care would have to be taken when setting up these counters.

The second option would be to replace the scintillators with Cerenkov detectors which are not sensitive to 0 degree pairs. This could , in principle, reduce the trigger rate by a factor of over 100.

The H×V counters would be replaced by triggers from the Hadron Calorimetry. By changing the Hadron Calorimeter from a gas detector to a scintillator readout (see hadron calorimeter section) it will become easy to generate a fast energy sum. Again this would drastically reduce the Master Gate rate. We intend to partially test this idea in the 1991 run by moving part of the H×V array behind the Inner Electromagnetic Calorimeter.

3.2 Microstrip Detector

The microstrip vertex detector is the E687 spectrometer's most important device for disentangling charm events from the very large backgrounds. It is installed in the region between the target and the first analysis magnet (M1) and consists of twelve microstrip planes, grouped in four stations of three detectors

each, measuring three coordinates at 135, 45 and 90 degrees with respect to the horizontal axis of the spectrometer.

The innermost central region of the system, covering the very forward production cone, has a resolution two times better than the outer region. The first station,which is the most crucial in determining the extrapolated error to the production point in the target, has twice the position accuracy of the other stations.

Each strip is read out by means of a front-end preamplifier, a remote-end amplifier and a charge integrating FLASH ADC. The analog signal at the amplifier output has a semigaussian shape with a base width of 100-120 ns. In the 1990 run the integration time in the ADC was fixed at 130 ns, giving a signal to noise ratio of about 17 for a single minimum ionizing particle. With a flux of about 10^7 electrons/sec on a 20% Pb radiator and a 10% Be target, about 8% of the events had embedded e^+e^- tracks. These embedded pairs were due either to more than one particle in the same RF bucket or particles from adjacent buckets. The vertex detector sees a pair mainly as a single track at 0 degrees not associated with the production vertex and having a pulse height consistent with 2 minimum ionizing particles.

The overall detection efficiency of every plane is $> 99\%$. The extrapolated transverse error to the mean interaction point in the target (placed 7 cm upstream of the first microstrip plane) is about 9 microns. The efficiency of the reconstruction code is 96%, on the average, for the tracks of $D\bar{D}$ events, including multiple scattering effects; contamination of spurious tracks is about 2.7%.

In order to face the increased photon flux we are considering two upgrades for the Microstrip vertex detector. One upgrade involves speeding up the analog electronics in preparation for higher incident photon flux and the second concerns reducing by 1/3 the detector thickness to minimize the effects of multiple Coulomb scattering.

3.2.1 Electronics upgrade

The present rate capability of the microvertex detector is limited by the duration of the analog signal at the input of the ADC's, which is about 130 nsec. When operating the Microvertex system at a e^+e^- rate higher than 5 MHz, as foreseen for the upgraded experiment, the probability for an out-of-time signal to be partly intercepted by the ADC gate would be very high(80%). To avoid contamination of out-of-time events the shaping time of the analog signal has to be reduced. This process could be accomplished by replacing the analog electronics with a faster electronics, but, at the same time, it would require a complete substitution of the cables connecting the preamplifiers, in the experimental hall, to the amplifiers, in the counting room. The new cables should propagate signals with very short rise times, in the range of 20-25 nsec. As a consequence this solution would be very expensive and time consuming and will be considered

as a the last resort. We think that the best solution is to utilize the fact that, while the instantaneous rate over the whole detector is very high, the rate on an individual strip is low and does not cause any significant pile-up of signals even with the present electronics. Thus we could simply reduce the time width of the signals from the amplifiers without reducing the intrinsic filtering time of the amplifiers. The analog information could be compressed into the charge and the time position of a delta function. Another possibility would preserve all the present electronics and split the outputs of the amplifiers to the ADC's and to a parallel array of constant fraction discriminators; their outputs would be latched only by the right trigger and the out-of-time signals could be eliminated by comparing the pattern of the ADC outputs with that of the constant-fraction discriminators. These solutions are currently under investigation.

3.2.2 Thickness reduction

The thickness of the microstrip detectors could be reduced from the present value of 300 microns to 200 microns with a corresponding reduction of the multiple Coulomb scattering error. (such thinner detectors are already commercially available). This reduction in thickness would improve the track reconstruction, reduce the vertex position uncertainty, and lower the e^+e^- pair rate in the spectrometer.

3.3 Enhanced Vertex tracking

Short-lived secondary decays could be more easily separated from the primary interaction if additional tracking information close to primary interaction was available. Two different ideas have been discussed. One idea is to install a pixel device upstream of the microstrip system and immediately downstream of the Beryllium target. Such a device would help in tracking a charged charmed parent or would help in identifying the parent as neutral. An alternate scheme would be to install 10 micron pitch silicon detectors at the end of the target.

3.4 Proportional Wire System

The proportional wire system has three planes in each station that are perpendicular (Y) or nearly perpendicular (U,V) to the bend plane. If no changes are made, the PWC's will have to operate at 5 times the current draw they ran at in E687. Experience with the chambers suggests that this would not be possible. We will exploit the fact that nearly all (greater than 90%) of the current draw occurs within a narrow region around the beam and is due to e^+e^- pair production in the target and in the material of the spectrometer. The beam size is about ± 2 cm at the tails. The e^+e^- pairs are spread out in a vertical swath by the action of the first analysis magnet. The second magnet recombines the pairs so that they form a fairly small spot at the last PWC,

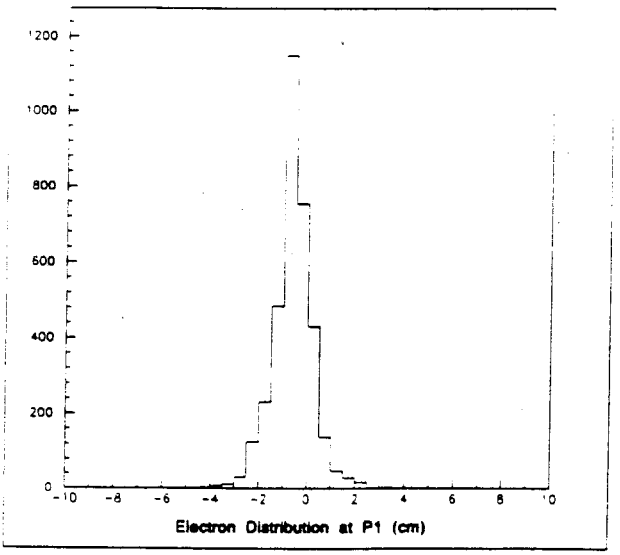

Figure 14: Pair distribution at chamber plane P1

P4. The recombination is not perfect because of bremsstrahlung energy loss by electrons and positrons in the material of the spectrometer. Pairs generated by photons interacting after the beginning of M1 are also not properly recombined and populate a much larger vertical swath at P4. The parts of the chambers outside the pair region will be able to handle the increased rate but we plan to deaden this central region. Figure 14 shows the distribution of hits from our 'pair' trigger at the chamber P1. The rates after the second magnet are such that deadening is unnecessary for P3 and P4.

There are several ways to deaden the pair region in P0, P1, and P2. The one that seems most promising to us was invented at Saclay and has been used extensively by E771 at Fermilab. Extra thickness of copper or silver is electroplated onto the sense wires in the region that is to be deadened. The extra thickness lowers the gain of the wire. This has been used on wires as thin as 0.6 mil. Our planes are 0.8 mil (P0) and 1.0 mil (P1,P2). Deadened regions can be produced with complicated shapes using this technique.

If we were to simply deaden the middle 4 cm of the spectrometer in X over the full height of the chamber, ± 115 cm, we would loose some charm events. By simply taking a sample of reconstructed $D^{\pm}$ mesons and asking how many had tracks that crossed the pair (deadened) region in P0,P1, OR P2, we find that we lose about 10% of our events. We therefore wish to recover the deadened region by instrumenting it with systems that can more easily withstand the high rate of pairs. In the horizontal coordinate this is simple. We plan to cover the deadened region with a small array of straw tubes. There will be two layers of overlapped 4mm diameter tubes. The vertical coordinates in this region will be measured by two new views of straw tubes. They will be angled at $\pm 45°$. Each view will be a double layer of 4mm straws and will cover the deadened area. The total number of straws is about 4500. These tubes will be instrumented with preamps and good amplifier/discriminators so they will be able to withstand the

high rates. One advantage of this system is that if a wire breaks or a whisker grows in a tube, the tube can be disconnected easily from the system. The straw tubes add 1.4% multiple scattering to the detector. They will need only latches for readout.

In addition to covering the deadened region, these planes will give us two whole new projections in the front of the system and will strengthen all aspects of our tracking, including the region outside of the deadened zone. The steep angle with respect to the other planes will improve the matching of all views significantly.

The alternative, a small system of 45° tubes to cover just the pair region, looks less desirable. The electronics and cable requirements are the same and the support is more of a problem. They provide no help outside the pair region.

We are studying the question of whether 6mm straws would be adequate for the planes stationed near the chambers P1 and P2. This would lower the channel count by about 1000. It may also make sense to drop coverage of the extreme corners of the aperture. This would also lower the channel count another 1000.

Finally, we can improve the rate performance, as well as the overall reliability and performance of the whole system by making certain improvements that will lower the gain at which we must operate the existing E687 chambers. These improvements were employed on the PWC P4 which was rebuilt between the 1987/88 and 1990 run. These improvements used all experience gained from operating the system during the first run. They included:

- Employing 3.3 mm pitch for the anode wires instead of the original 3 mm pitch for P1 and P2 . The rebuilt P4 used 3.3 mm pitch. This permitted us to lower the voltage by 200 volts for the same gas gain. The integrated mass resolution of the system was hardly affected by this change and the chamber achieved higher efficiency than any other chamber in the experiment.

- Modifying the gas box for P0, P1, P2, and P3 so that signals are fed to the outside through header pins as they are in the modified P4. In the original design, cables run through slits from the inside to the outside of the gas box. The cables are sealed with RTV. The modified P4 had the lowest gas leak rate of any of the chambers. The noise was also lowest for this chamber although we cannot really claim that this was related to the modified gas box. Whatever the cause, P4 ran at the lowest threshold of any plane which permits reduced gas gain.

- We would like to redo the sense and high voltage planes using the 'machine planing' method that was used to get a tolerance of ± 1.5 mils for P4's gap. When the gap is uniform, all parts of the chamber plateau at the same voltage and this obviously produces the best running condition.

- We would like to redo the artwork of the high voltage planes for at least P1 and P2 using the 'longer' high voltage pads that were employed for

P4. The major reliability problem we encountered with the PWC's was that occasionally a spark, trip, or other upset would cause a high voltage wire to come lose. Almost all such wires were at the edge of a cathode pad (16 wires ran to each pad). It was hard to get enough solder on the edge wires to make a secure contact. By making the pads much longer in the direction of the wire, this problem was completely eliminated in P4.

- We want to replace the 'ancient' amplifier discriminators on the chambers P0 and P3 with the more modern ones used on the other chambers. These planes suffered from oscillation problems. The method for doing this was used in the 1987/88 run and is well understood.

These improvements should allow us to lower the threshold and the voltage and help sustain higher fluxes. they should also reduce the downtime from chamber problems in the experiment which, while small, was not negligible.

This is a somewhat 'belt-and-suspenders' approach to a problem which can make or break the experiment. The chambers have to work. If we can improve them enough so deadening is not an issue, that would be excellent but we have no way of being certain of that so we wish to embark on the straw tube construction as well.

Finally, we will explore the use of preamps and the use of gas mixtures other than 65-35 argon-ethane. Rate capability will be a major concern here.

3.5 Muon detectors

3.5.1 Inner Muon Detector

The inner muon system used in E687 consists of several coarser granularity scintillator hodoscope and 4 arrays of 5 cm diameter proportional tubes. The muon proportional tube system provided the high granularity position information required to match the muon hits to the proper track measured in the upstream spectrometer. The scintillation counter array was used for muon triggering and confirming the muon identification by providing additional coincidences. We intend to augment the existing E687 inner muon system with a relatively fine granularity x & y scintillator hodoscope placed just downstream of the hadrometer. There are two motivations for this proposed upgrade.

- The use of scintillator allows for a very tight (1 RF bucket) latch which should perform better than the muon proportional tube system (which required a roughly 1 μs readout time) given the higher rates envisioned in P831. Because of the superior time resolution of scintillator, the proposed new hodoscope should should significantly reduce potential muon backgrounds due to halo muons.

- The upstream placement of this hodoscope should significantly (by factors of 5) improve our ability to match hits in the muon system to tracks

measured in the upstream spectrometer by significantly reducing the lever arm for multiple coulomb scattering by the hadrometer.

Given our multiple scattering environment, calculations indicate that 4 cm wide scintillation counters provide good position resolution over the muon momentum range(10 GeV $< P_\mu <$ 50 GeV) relevant for semileptonic charm decay. In order to achieve single RF bucket timing resolution, we are restricted to using a maximum optical path of less than 3 meters. Since we must span a transverse area of 2 meters by 3 meters, the natural solution is to use two spans (of 1.5 meters or 1 meter) to cover the full horizontal and vertical aperture. Hence a total of 250 scintillation counters will be required to construct this hodoscope.

The virtue of a fine granularity system is likely to be a simplicity in the light collection system since the counters are by necessity fairly narrow. For example, we have considered reading out each of the 250 hodoscope elements consisting of 1 cm thick scintillator by an individual 25 mm diameter photomultiplier tubes optically coupled directly to one end (without adiabatic light guides). Under these conditions, a large enough number of photoelectrons (several hundred) should be collected per minimum ionizing particle thus allowing the use of commercial fast discriminators and modest gain photomultiplier tubes.

We are presently studying the possibility of backing up the 4 cm wide hodoscope with a much coarser grain (16 cm wide) hodoscope placed downstream of the second slab of muon steel. The better filtered coarse array, would serve to both confirm the identification provided by the upstream array (with even more hadronic absorption), and serve as a backup to match upstream tracks for those events where the upstream array is confused by hadronic shower leakage or δ- rays.

3.5.2 Outer Muon Detectors

The outer muon system is located directly behind the yoke of M2 and consists of two scintillator arrays and two proportional tube arrays. The scintillators are used for triggering while the proportional tubes are used to associate the muon "hit" with the wire chamber tracks. As in the inner muon system, the outer muon proportional tubes will be too slow to handle the anticipated rates and must be replaced. We are presently considering two options to replace the proportional tubes.

The first option involves building an outer scintillator array with 5cm wide strips that has adequate granularity for matching the muon tracks. This design would be similar to the proposed inner muon array. The second option involves reconfiguring the existing outer muon scintillators. The reconfiguring would involve additional light guides and phototubes to achieve an acceptable muon hit efficiency. The advantage of the second option is that the detector would require less space. In both designs an additional 300 new photomultiplier tubes and bases would be required.

3.6 Hadron Calorimeter

The hadron calorimeter for E831 has to perform the following functions, ordered by priority:

1. Provide a fast trigger decision based on total hadronic energy. This trigger decision must be available in time for the Level I trigger to avoid substantial Level II deadtime. The trigger must be formed in about 100-150 ns.

2. Provide a possible second level trigger based on total E_{perp}. This kind of trigger has been used by E691 and others to achieve a factor of 2-3 reduction in trigger rate while being about 80% efficient for charm. Our own simulation demonstrates similar results.

3. Provide measurement of the position and energy of neutral showers.

The first item is crucial to the success of the experiment. The second item would be a very useful option for reducing the total amount of data recorded. The third item, neutral shower reconstruction, would be a nice addition to the experiment and would allow access to some interesting states containing neutrons, K^0's, and Σ's, if it worked well, but is not critical to achieving the main goals of the experiment.

The present gas/proportional tube hadrometer produces pulses that are 800 ns long. This makes it unusable in the Level I trigger. (In the lower rates of E687, it was possible to use the hadrometer information in the second level trigger so this was not a problem).

A calorimeter based on scintillator meets these requirements. We have investigated two designs: scintillator strips and scintillating tiles. Figure 15 shows a possible tile arrangement. The best arrangement will be determined from a detailed simulation of the E_{perp} trigger.

At present, we favor the tile design over the (long) strips for the following reasons:

- The mounting scheme is much easier. In particular, the need for both X and Y readout for the E_{perp} trigger will be difficult (although not impossible) to do in a strip geometry.

- Light attenuation corrections are practically negligible for the tile geometry as compared to the long strips. This is especially important for the use of the device in the Level I trigger, where there is no time to correct for attenuation. Even in the Level II trigger, it simplifies the electronics if it is unnecessary to make large corrections.

- It is possible to achieve much better segmentation with the tiles, which is useful for both the Level II trigger and for the reconstruction of neutral showers. The offline shower reconstruction is much simpler with a pad/tower geometry.

The biggest drawback to our use of the tile design is that we haven't built anything like it before. We have discussed the tile calorimeter with many people at Fermilab who are actively involved in developing this technology and are convinced that enough is known so that we can be confident that we can construct such a device and that it will meet all our requirements.

The device that we have simulated uses the steel plates from the existing E687 hadron calorimeter, which has 28 1.75" thick plates. We would place planes of 2 cm thick scintillating tiles between these plates. The expected energy resolution for this system is $\frac{75\%}{\sqrt{E}}$. With the segmentation shown in the figure each plane will have 88 tiles. The tiles would be ganged into 3 or 4 towers longitudinally. In the scheme we have modelled, the signals from plates 1-5, 6-9, 10-14, and 15-28 were ganged together. Each longitudinal sample then has about the same energy deposition for the 125 GeV tracks striking the calorimeter. The total number of readout channels (PMTs going to ADC's) is 352. This is to be compared with 570 channels in the existing E687 calorimeter.

The light from the tiles will be collected by fibers inserted into machined grooves in the tiles. The design is copied from the CDF/SDC tests. The main difference is that we are using thicker scintillator and larger size tiles than that group used. We will have to perform a test to see how the signals scale with tile thickness and area. The result might influence the number or arrangement of fibers within the tiles.

The Level I trigger is formed by adding the the pulses in groups, whose duration is about 20 ns, integrating them, digitizing them, and converting them to a level. The levels from various sectors are then added and sent to a flash adc. The digital output is compared to one (or more) thresholds. This can easily been done in 100-150 ns available.

Only preliminary studies of the use of this device in the Level II trigger have been carried out. The final pad geometry and and the longitudinal segmentation are not yet worked out. The biggest problem, as we see it, is to include the information on the E_{perp} from the nearly 2000 channels of electromagnetic calorimetry into the summation.

We have also done a comparative cost analysis of the tile and strip geometries. The costs for materials, photomultipliers, electronics, cables, triggers, etc are about the same. The labor costs for the tile system are harder for us to estimate and we have drawn heavily on experience from CDF/SDC prototype development. The costs of the two systems are not significantly different.

3.7 Beam Instrumentation and Flux Monitors

After radiating photons in the lead radiator (27% X_o for E-687), the recoiling electrons and positrons are detected in a series of electromagnetic shower hodoscope detectors.[39] See Figure 16. In order to account for the coincident multiple bremsstrahlung photons emitted by a single electron, a Beam Gamma Monitor (BGM) electromagnetic shower detector is placed in the zero degree

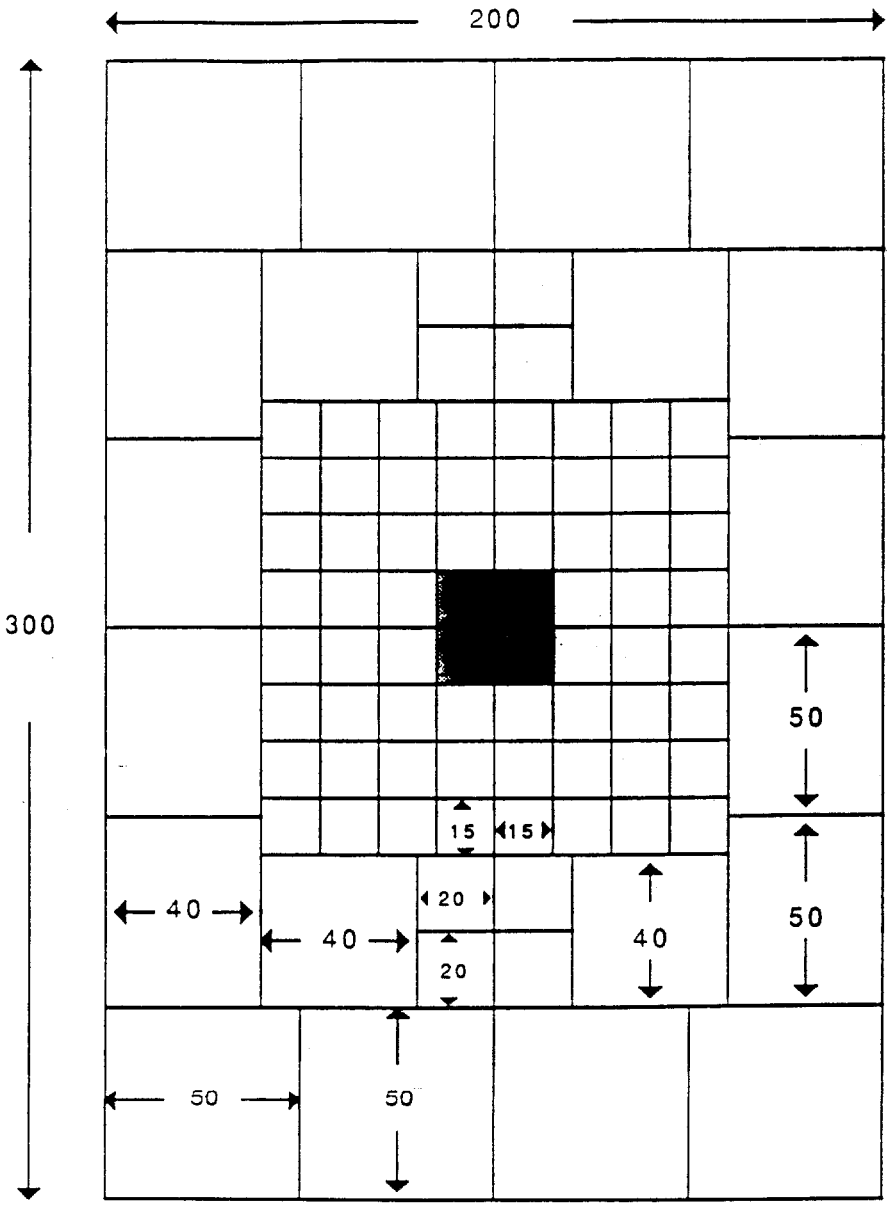

Dimensions in cm

Figure 15: Transverse segmentation of proposed tile calorimeter

photon beam at the downstream end of the spectrometer. In order to get the energy of the photon initiating the hadronic event, the additional multi-bremsstrahlung energy in BGM was subtracted from the tagged electron (or positron) energy loss on an event by event basis. BGM was also used to measure the incident photon flux. The silicon microstrip-based incident beam momentum tagging system[40] measured the momentum of each incident electron or positron.

Experience during the previous E-687 runs has indicated that care must be taken in preparing for the increased beam intensity and luminosity proposed for P-831. In addition, there are some obvious upgrades that will also improve the performance, triggering, and data analysis for P-831.

The ability to accurately measure and to monitor the incident photon kinematics benefits the study of most of the physics topics of P-831. However, many physics topics such as charm particle spectroscopy, relative branching fractions, and Dalitz plot analysis can be accomplished without explicit knowledge of an individual photon energy. The measurement of the photon energy on an event by event basis, the overall photon energy distributions, and flux normalization are vital to studies involving cross sections and production dynamics.

3.7.1 Higher Luminosity Issues

During the 1990 and 1991 Fixed Target Physics running periods, E-687 ran successfully at sustained average incident rates of 10^7 electrons per second. Dividing by the 53 MHz RF structure and multiplying by a factor of 3 to account for both the gross and fine time structures in the beam, this corresponded to an average electron occupancy of 0.6 per RF bucket. Pile-up from random coincidences was starting to become bothersome. For P-831, we propose to run at a factor of 5 higher instantaneous rate, giving average electron occupancies up to 3.0 per RF bucket!

There are three distinct classes of pileup: (1) DC or slowly varying baseline shifts due to the overall rate or very long tails of distributions, (2) adjacent RF bucket interferences, due to instrumental resolving times or signal tails of the scale of a few RF bucket spacings in time, and (3) multiple incident electrons coincident within the same RF bucket, within 1 nsec of each other. It is assumed class (1) can be cured by just very hard analog work and class (2) can be cured by improving the signal crispness and timing characteristics and reducing the coincidence resolving times. Pileup class (3), however, represents an irreducible challenge, requiring new types of hardware, rather than simply speeding up that already existing in E-687.

We assume that we will be able to procure ADCs and Coincidence Registers that can be made to work efficiently at 53 MHz single bucket resolution (18 nsec gating) and adjacent bucket double pulse rejection for the existing BGM, RESH, and POSH systems, as well as for possible electron and positron trajectory tracking systems.

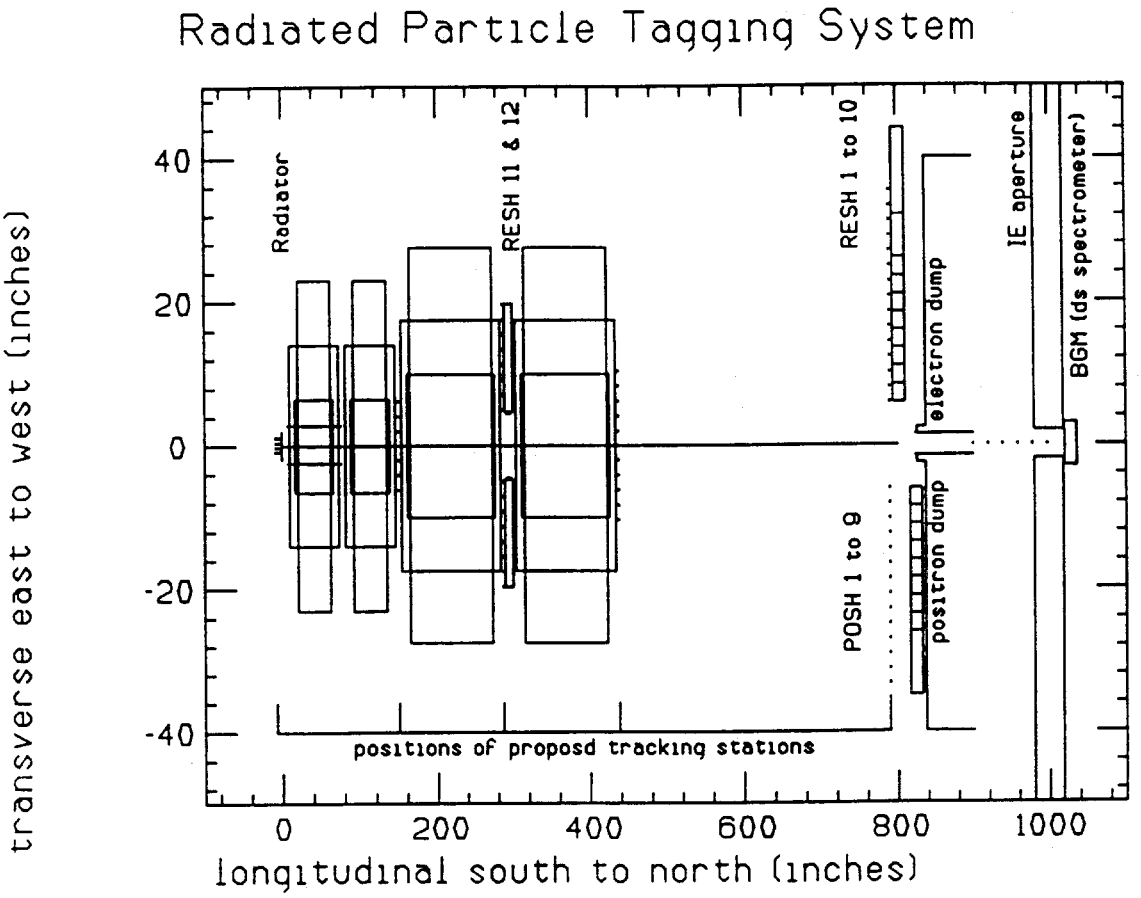

Figure 16: Existing Radiated Particle Spectrometer (including BGM). The positions of proposed additional tracking planes are indicated.

BGM

The BGM counter was a conventional lead + polyvinyltoluene scintillator (Pilot B) electromagnetic shower calorimeter. In effect, it was the photon beam dump. In order to minimize radiation damage, it was operated in a nitrogen atmosphere. Over the course of the 1990 FT run, it did suffer 15% signal degradation about the central beam position. Scaling by the increased luminosity expected, or even by logarithm of luminosity, would indicate that we are headed for trouble. The most troublesome aspect of the radiation damage proved not to be the magnitude, but its spatial distribution. The radiation damage followed the spatial distribution of the photons. Without position resolution, it was impossible to tell where the shower occurred and therefore to correctly estimate the detector gain response. This was the limiting factor for the photon energy resolution.

Possible solutions for investigation include an easily replaceable liquid scintillator (if a sufficiently fast one can be found), incorporating the BGM in a pressure vessel to allow clearing with high pressure O_2 (a slow process, at best), more radiation resistant scintillators, possibly scintillating fibers, or shower position readout to monitor the radiation damage and correct for the reduced detector response on an event-by-event basis.

Pileup due to occupancies of nearby buckets could be monitored and corrected with BGM analog fanout capability and dedicating additional ADC channels to measure the energy deposition for nearby RF buckets. The BGM gain monitor (a QVT-based stand-alone data acquisition system) will be triggered by an individual RESH logic bit(s) giving monochromatic tagged energy spectrum line(s). This will be much easier to monitor rather than the photon continuum end-point energy, especially in an environment with substantial pileup in the same RF bucket.

The BGM also served as an important Luminosity Monitor for the experiment.[41] Previously, this application was based on simply counting the number of photons above some discriminator threshold, typically above 100 GeV. This digital counting method breaks down when the instantaneous intensity gets too high or incident electron occupancies approach 1 per RF bucket. Since this is very definitely expected to occur for P-831, another approach such as a Wilson quantameter [42] could be employed. A simple hybrid of interspersing a few (thin) integrating ionization chambers, every 3 X_o or so, within the scintillation calorimeter seems promising.

RESH and POSH

The existing recoil spectrometer for the radiated electrons and positrons (Figure 16) is based on lead-lucite and lead-scintillator EM shower calorimeter detectors used to identify electrons and positron by correlating deposited energy with the momentum dispersion of the tagging dipoles. The position at the RESH and POSH arrays can be quickly decoded by discriminator bit patterns and can be further refined by analyzing the energy sharing between adjacent RESH or POSH counters. The on-line Level II event trigger required a RESH

or POSH hit pattern consistant with only one electron or positron. Events with extra discriminator hits were vetoed. However patterns consistant with TWO electrons hitting the same RESH or POSH elements were accepted for later rejection by pulse height analysis.

A serious question for the operation of RESH and POSH concerns how greedy one wishes to be in striving to pick up LOWER energy tagged photons. These are closer to the beam giving higher rates in the innermost counters, gain changes due to radiation damage, and poorer photon energy resolution due to the reduced spatial dispersion.

These systems, both logical and analog, need to work at the 53 MHz RF rate. This will require some work in improving the optimization of the analog signals through photomultiplier bases, amplifiers, cables, delays, noise suppression, etc. Even the digital pulses, discriminated locally near RESH and POSH, suffered from drive capability and cable dispersions to be a problem in setting and maintaining the efficiency of the logic and trigger system. This could be greatly alleviated by the introduction of higher performance CAMAC coincidence registers whose timing performance will depend mainly on the gating signal and not strongly depend on the characteristics of the signal shapes for each individual channel. Additional dedicated RESH-POSH trigger logic calibration (frequent automated delay curves) and monitoring fanouts and scalers would be appreciated.

The RESH and POSH triggers for E-687 required simply more than about 20% of the nominal energy deposition in a given single counter. This provided adequate trigger selection since those counters with E/P = 20% were, in fact, almost always adjacent to another counter with E/P = 80%. Especially with the non-negligble hadronic background in the positron beam, we may desire to tighten up the E/P trigger logic requirements, both on the low end to reject hadrons and on the high end to reject two electrons or positrons hitting the same counter. Since the size of highest rate RESH and POSH detectors is approximately 2/3 the transverse size of the EM shower, forming analog sum pairs such as 1+2, 2+3, 3+4, ...(i-1)+i will insure total energy containment (E/P close to 1) for triggering with tight thresholds.

Although it would be desirable to have functioning veto shower counters within the electron and positron dumps, in E-687 it has proven difficult to keep them from dying from radiation damage within a few days. Such beam vetoes would be especially helpful to reject events in which an electron experiences a small energy loss in the radiator, not enough to be swept into RESH, but the photon converts in the radiator and hits either RESH or POSH (cross-vetoes will not allow both RESH and POSH hits) and gives a false tag with minimal energy hitting the experiment target.

3.7.2 Additional Features for Improved Performance

By improved performance, we mean not only improved resolution and physics capability, but also ease of operation, monitoring, calibrating, and analysing. Some of these proposed improvements, such as easier timing curves, gain monitoring, vetoes, etc., have already been mentioned in the Luminosity Upgrade Section. The possibilty of actually tracking the radiated electron and positron trajectories will not only enhance photon energy resolutions, but also improve primary vertex localization analysis methods, and help facilitate the full use of the silicon incident beam tagging spectrometer for events with more than one incident electron or positron per RF bucket.

Recoil Electron and Positron Tracking

Currently, the horizontal electron (and positron) trajectories are measured about the last horizontal bend in the incident electron beamline.[40] This gives the incident electron momentum before radiating. In order to get optimal resolution of the radiated electron and positron tagging spectrometer, it is desirable to know the trajectory of the projected electron from the radiator, past the RESH and POSH detectors, to the experiment target. The interacting photon position at the target is measured by spectrometer vertex silicon microstrip detector system, to an accuracy of a few microns in three dimensions. The horizontal position of the electron at the radiator could be projected using the beam tag track traced though the last stage triplet focussing quadrupole magnets. Continuing to the target has shown that a resolution in matching the projected electron trajectory to the reconstructed vertex position of $\sigma_x = 3$ mm is attainable. Another horizontal tracking plane at the radiator capable of withstanding high rates, would better pin down the projected electron (and photon) trajectory even better. This would greatly improve the resolution of the radiated electron spectrometer. In addition, the projected horizontal trajectory could then serve as a road for searching for primary event verticies, much as incident beam silicon hodoscopes for hadron experiments.

If we also add a vertical position detector at the radiator, we can then correlate the event vertex position with the position of the incident electron at radiator and get both horizontal and vertical photon directions and event production angles. This may be interesting for some exclusive physics such as the study of photoproduction of vector mesons.

So far, we have only discussed single electrons or positrons per RF bucket. The beam tagging silicon spectrometer is capable of reconstructing more than one track per RF bucket (up to five!). The problem is in determining which of these tracks actually radiated the photon in question. Since we are using a thick (27% Xo) radiator, the flip answer is that all of the electrons radiated! If we have, for example two electrons reconstructed in the beam and one in the RESH, we would have to do some TRACKING in the radiated particle spectrometer to disentangle. This could be either horizontal (large aperture requiring many detector elements) or vertical (smaller aperture, scaled to the vertical beam size,

Table 9: Multiple Scattering in Radiator Projected to Target

k_{photon} GeV	e' GeV	σ_y mm
100	150	0.67
150	100	0.92
200	50	1.75

rather than the horizontally dispersed radiated beam size). So far, we have only considered the vertical tracking option.

A simple calculation has shown that a useful projected vertical (or horizontal) trajectory attainable from such a radiated particle spectrometer would require a resolution with σ_y less than about 1 mm. This would allow disentangling the pair conversions in the target from photons from multiple incident electrons with a high degree of reliability. This would also form a useful road-width seed for primary vertex reconstruction algorithms. Finally, this resolution is about what is expected for multiple scattering of the incident and radiated electron in the thick radiator. Therefore, there is no justification for attempting any finer resolution.

The multiple scattering in the radiator can be simply modelled by considering, on the average, two radiators, each of 1/2 thickness. The incident 250 GeV electron scatters in the first. The radiated electron, whose energy depends on the photon radiated, scatters in the second section. This gives the vertical resolution projected to the target due to multiple scattering in the radiator as a function of the photon energy. This simple model will have to be further refined before designs for this tracking system are finalized.

In order to obtain this spectrometer resolution of $\sigma_y = 1$ mm, we would require vertical detector elements of 1.5 mm size at the radiator, at the exit from the last tagging dipole, and at the RESH and POSH detector planes. In addition, if we desired to vertically tag for particles that only hit RESH12 and POSH12, we would require 0.75 mm detector elements between the second and third tagging elements and at the RESH12 and POSH12 detector planes. In addition, the vertical detector elements at the radiator would have to be reduced to 0.75 mm size also. This is due to the reduced lever arm and the more upstream position of RESH12/POSH12 relative to the main RESH and POSH arrays. Adding the two additional upstream stations in the tracking reconstruction algorithm for particles that reach the main RESH/POSH arrays adds little gain to the overall resolution.

Finally, there would be one or two slanted planes (1.5 mm element size) at the radiator, coupling the horizontal and vertical views and allowing the correlation of the multiple horizontally momentum measured tracks with the vertical trajectory of the electron or positron giving the RESH or POSH trigger.

This system would require the addition of the following stations, element sizes, and channel counts:

Station-view	Element Size	Number of Elements	V x H Size
Radiator-x	0.75 mm	64	5 cm x 5 cm
Radiator-y	0.75 mm	64	5 cm x 5 cm
Radiator-u	1.5 mm	64	5 cm x 5 cm
Radiator-v	1.5 mm	64	5 cm x 5 cm
M2-M3 - y	0.75 mm	2 x 64	5 cm x 12.5 cm
RESH12-y	0.75 mm	2 x 64	5 cm x 37.5 cm
M4 ds - y	1.5 mm	2 x 32	5 cm x 25 cm
RESH-y	1.5 mm	2 x 32	5 cm x 75 cm
Totals	0.75 mm	384	
Totals	1.5 mm	186	
Grand Total		576	

These detectors could be silicon microstrips at the radiator (but watch the additional multiple scattering), overlapping layers of scintillating fibers (can be fairly thick for adequate number of photoelectrons) with multi-anode photomultiplier readout, or any other detector giving adequate resolution and single RF bucket timimg. The resolutions and geometric area coverage for those detectors downstream of the radiator look about ideal for straw tubes. However, taking 4 mm (minimum?) diameter straw tubes, the maximum charge collection time would be on the order of 70 nsec or 4 RF buckets (drift velocity of about 3 cm/μ-sec in $Ar - C0_2$). These straws would cover only the aperture of the RESH and POSH arrays, so would not have to respond to every incident beam particle. Multiple layers of straw tubes per station and multi-hit TDCs appear to be able to provide adequate time resolution to perform the multi-RF bucket pattern recognition.

Once we do have the trajectories to determine the momentum of each of the two or more incident electrons and determined which electron actually struck the RESH, we know the energy loss and photon spectrum for that identified electron. However, there still remains the additional radiation from the other electron(s) that will be producing confusion due to additional photons striking BGM but not correlated with our identified tagged electron. In fact, the average electron or positron incident upon the radiator would deposit approximately 1/4 of its energy in BGM, yet still not be detected in either RESH or POSH. We still must understand how to deal with such BGM pileup.

Finally, we may desire to have better position resolution in front of our large momentum bite detectors such as RESH1, RESH2, POSH1, POSH2, RESH12, and POSH12. Either finer granulariy shower counters or position hodoscopes could be considered.

3.7.3 Event Cleanliness

Additional hardware will be investigated to improve event tagging cleanliness. The analog sum E/P = 1 trigger described above will reduce hadronic and multiple radiated electrons or positrons per event. The beam dump counters RESH0 and POSH0 to veto the false tag triggers due to second order processes involving minimally-radiated electrons or positrons will be difficult to keep alive at the proposed electron beam intensities. Similarly, there has been preliminary studies performed by E-774 in this beamline of electron identification by synchrotron radiation tagging. In principle, this could detect the presence of protons, the main hadronic background in the positron beam. However, the phase space of the electron and positron beams make problematic the optimal placement of synchrotron radiation detectors close enough to the beams. It is also difficult to imagine how a veto can operate efficiently on a "NO" or lack of signal in coincidence with one or two positive "YES" signals in the same RF bucket. Still much more thinking, research, and development are needed.

3.8 Triggering

The triggering strategy will have to be changed in this experiment. Previously our group has always tried to write out all hadronic events on-line and then sort out the good events in software where more information is available (such as the number of charged tracks in the silicon microstrip). Rates will now be high enough to require that fast decisions need to be made during data-taking.

The e^+e^- pair rate is expected to be $5MHz$ with a hadronic rate of $5kHz$. As explained in the trigger counters section the hadron calorimeter is being incorporated into the Level I trigger. It is assumed that essentially all pairs are removed by the Level I trigger and that the surviving events are more than 80% hadronic. However the hadronic rate is such that we will need to reduce it by a factor of 4 before events can be written to tape.

We plan to implement a combination of photon energy and track multiplicity to get rid of events initiated by low energy photons (which have very low charm cross section) or events which come from primarily soft scattering processes. This will result in a reduction of at least a factor of two.

A final factor of at least 2 will be achieved by using an E_{perp} trigger formed of information from the Inner Electromagnetic Calorimeter, the Outer Electromagnetic Calorimeter and the Hadron Calorimeter. This trigger is very similar to the trigger used by E691. In that experiment a factor of 2.5 was gained in the charm to hadron ratio. This E_{perp} trigger is presently being studied. Studies performed at Breckenridge and at Snowmass indicated that much larger improvement factors could, in fact, be made.

3.9 Data Acquisition

The problems of triggering and data-acquisition (DAQ) are closely related: the better the trigger, the lower the requirements on the DAQ. We assume that the combination of the first and second level triggers will produce a total of 25,000 events per spill which need to be read in. The average event size is 3 kilobytes so the total amount of data is 75 megabytes per spill.

The following is the organization of the present E687 DAQ:

- Front-end digitizing electronics. This consists of five data streams: Microstrip detector ADC's designed by Milan, Lecroy 4290 TDC's with Fermilab readouts, Smart Crate Controller readout of Fermilab and Lecroy PCOS latches, and two Fastbus crates of Lecroy 1885 ADC's.

- Real-time data buffering. The data streams are read into separate 4 megabyte Lecroy 1892 Fastbus memories. The trigger must remain disabled while this transfer occurs, introducing dead time. The average readout time for each stream is summarized in table 10. Data rate requirements here are the stream data block sizes divided by the acceptable readout time.

- Spill buffering. A GPM Fastbus Master processor merges the data streams from the Fastbus memories into event records. Blocks of event records are transmitted by Branch Bus to a 60 megabyte spill memory buffer located in the PANDA VME crate. Data rate requirements here are the average total data per spill divided by the active 20 second spill time.

- Data recording. The data is recorded on up to four Exabyte 8200 8mm tape drives in parallel. Data rate requirements here are the average total data per spill divided by full 60 second spill cycle.

Some changes to the existing Data Acquisition system are required to meet the required five fold increase in data rate.

With about 1 millisecond between events, an acceptable 10% deadtime requires 100 μsec real time data buffering. Table 10 shows that the microstrip stream and the SCC latch stream need no revision. The ADC and TDC systems must read the data out at higher speeds.

There are several options for speeding up the TDC readout.

- Presently, the TDC readout time is limited by the speed and number of the readout controllers. Some speedup can be achieved by increasing the number of 'readout' controllers. However, for events with a very large number of hits (perhaps of electronic noise/oscillations), this does not necessarily solve the problem. The next option is to speed up the data transport within individual crates. This option is being investigated. It would require the design and construction of about 30 modified crate

Table 10: Average readout times for E687 data streams

Data Stream	readout time (μsec)
Microstrips	20
latches	50
TDC's	300-600
ADC (1)	1000
ADC (2)	1000

controllers and possibly some modifications to the TDC's themselves. We would have to do a systems test to confirm that the system really achieved the desired speed fairly soon in order to have confidence in this approach.

- The TDC system could be replaced by a new system such as the one designed by the Fermilab Physics Department. This system is now being tested and seems to work well. The readout speed meets our requirements. The cost is about \$35/channel and we need 13,500 channels of TDC.

- The TDC system could be replaced by latches. For the most part, we do not make much use of the timing information and the mass resolution is dominated in many cases by multiple scattering. The latches would be about 1/3 the price of the TDC's. Latch systems of the appropriate type might be available from existing electronics inventory.

The problem of speeding up the TDC readout is largely one of cost optimization. Several technical solutions are available.

P831 will have about 2800 channels of pulse height information, slightly less than E687. E687 used LeCroy 1885 Fastbus ADC's. The 1885 Fastbus ADC digitization time alone is nearly half a millisecond. It will therefore be necessary to use a different ADC system. There are commercial options available, such as the Lecroy FERA system, which would achieve the required speed. This system is quite expensive. There is a design for a Fastbus ADC by the Fermilab Physics department which has very fast readout speed and is suitable in all other ways for the experiment and which is estimated to cost less than \$75/channel. LeCroy is planning a new ADC, the 188X, which has much shorter digitization time and on-board pedestal suppression. It has suitable sensitivity and range for our needs. The cost per channel is projected at \$60-70/channel. Readout will take between 50 and 100 μsec. The device is now in the prototype stage and will be tested shortly at Fermilab. Assuming it lives up to its specifications, this would probably be the best choice.

The old E687 data buffering and logging system would be pushed to or beyond its limits in logging the nominal 1 Megabyte per second of data. The maximum event rate ever achieved in the event building stage was about 20,000 small events per spill, with a very large dead time.

We plan to simplify the system, using existing, proven modules in supported configurations. Front ends should be read out through standard RS-485 data cables. We would like to use a supported generic commercial workstation to perform event building, filtering, data logging, monitoring and run control. Realtime programs and special device drivers should not be required. We will continue the very successful practice of depending on Fermilab Computing Division software support for major elements of this system.

We will use VDAS memory buffers, originally developed by Fermilab for E687, to provide both real time and spill buffering. EBI modules provide a simple, inexpensive, and fast connection from VDAS to the VME bus of the data logging workstation. This technology also gives us the option of using the primary data paths for interspill calibrations. A memory module planned as part of the DART system will combine the VDAS and EBI functionality on a single VME card, and when available could replace the VDAS/EBI combination.

Data will be logged on 8mm tape using Exabyte 8500 double density tape drives. At half a megabyte per second per drive, we will log to two drives in parallel. Data logging rates can be increased by adding more drives to the output SCSI bus, or adding additional SCSI adaptors to the workstation. For short calibration runs, higher rate data logging to disk will be possible.

In conclusion, the DAQ can be upgraded with existing technology to operate at the required rate. If the trigger rate exceeds the target of 25,000/spill by a factor of two, the "downstream" portion of the system can handle the situation with no trouble. The "front-end" will produce a factor of two more deadtime, which will result in an increase from 10% to 20%, an acceptable situation.

4 Upgrades to Spectrometer to Improve Efficiency

Some part of the improvement in the charm and beauty yield are obtained by improving the efficiency of the spectrometer for reconstructing these events. These improvements are described in this section.

4.1 Cerenkov Counters

This section reviews the layout and performance of the present E687 Cerenkov system, and discusses a possible improvement for a new run. Our basic conclusion is that the existing system performs well for the charm physics of a new photoproduction run but we are studying a modification which might extend the capabilities of the experiment. The present E687 Cerenkov system consists of three multicell Cerenkov counters with different Cerenkov thresholds. Table 11 summarizes the cell count and thresholds for the existing Cerenkov system.

Low momentum (or wide angle) tracks which fail to traverse the M2 aperture are analysed by both C1 and C2; tracks which traverse the M2 aperture are

Table 11: Characteristics of the Čerenkov Counters

Counter	Gas	Threshold (GeV/c)			No. of Cells
		Pion	Kaon	Proton	
C1	HeN_2	8.4	29.6	56.4	90
C2	N_2O	4.5	16.2	30.9	110
C3	He	17.0	61.0	116.2	100

analyzed by all three counters. The existing Cerenkov system allows protons and kaons to be separated from pions over a momentum range of 4.5 GeV to to 61 GeV and provides unambiguous electron identification for momenta up to 17 GeV for tracks traversing the M2 aperture. We used pure helium in C3 in order to achieve the highest possible Cerenkov threshold available using an atmospheric pressure counter. The Cerenkov thresholds of C1 and C2 were matched to the C3 threshold to provide a continuous momentum range for particle identification (e.g. the kaon threshold of C1 matches the proton threshold of C2 and the proton threshold of C1 matches the kaon threshold of C3).

The present E687 Cerenkov counter system performed well in both the 1988 and 1990 run period. Figure 17 shows an inclusive, combined $D \rightarrow K\pi$,$K2\pi$,and $K3\pi$ signal obtained in our 1988 run with and without Cerenkov identification requirements on the kaon. About 60% of the total charm signal survives the Cerenkov cut. If one considers cases where the kaon traverses the M2 aperture and thus has a chance of being identified by C3, the kaon is Cerenkov identified as definite kaon or kaon/proton ambiguous about 70 % of the time. These identification fractions include the effects of Cerenkov confusion due to overlapping tracks as well as the effects of the finite Cerenkov identification momentum range. The good performance of the present Cerenkov system can also be confirmed through the decays $\phi \rightarrow K^+K^-$, $K_s \rightarrow \pi^+\pi^-$ and $\Lambda \rightarrow P\pi^-$. Roughly 80% of protons from Λ decays are identified as proton or kaon/proton ambiguous in our 1988 data.

The kaon identification range of the Cerenkov system performs well for most of the charm physics goals of E687. At present, both C2 and C3 have close to optimal performance with asymptotic photoelectron yields in excess of 8 photoelectrons. The photoelectron yield of C1 is about 3 photoelectrons primarily owing to its small physical length (only about 1.4 meters) and relatively high pion threshold (8.4 GeV). It might be possible to extend the C1 radiator length. A 2 foot extension would raise the photoelectron yield to about 4.3 photoelectrons. Extra photoelectrons would significantly solidify particle identification for the case of well isolated tracks. The penalty of a 2 foot extension would be a 40 % increase in the radius of Cerenkov light for each track which would

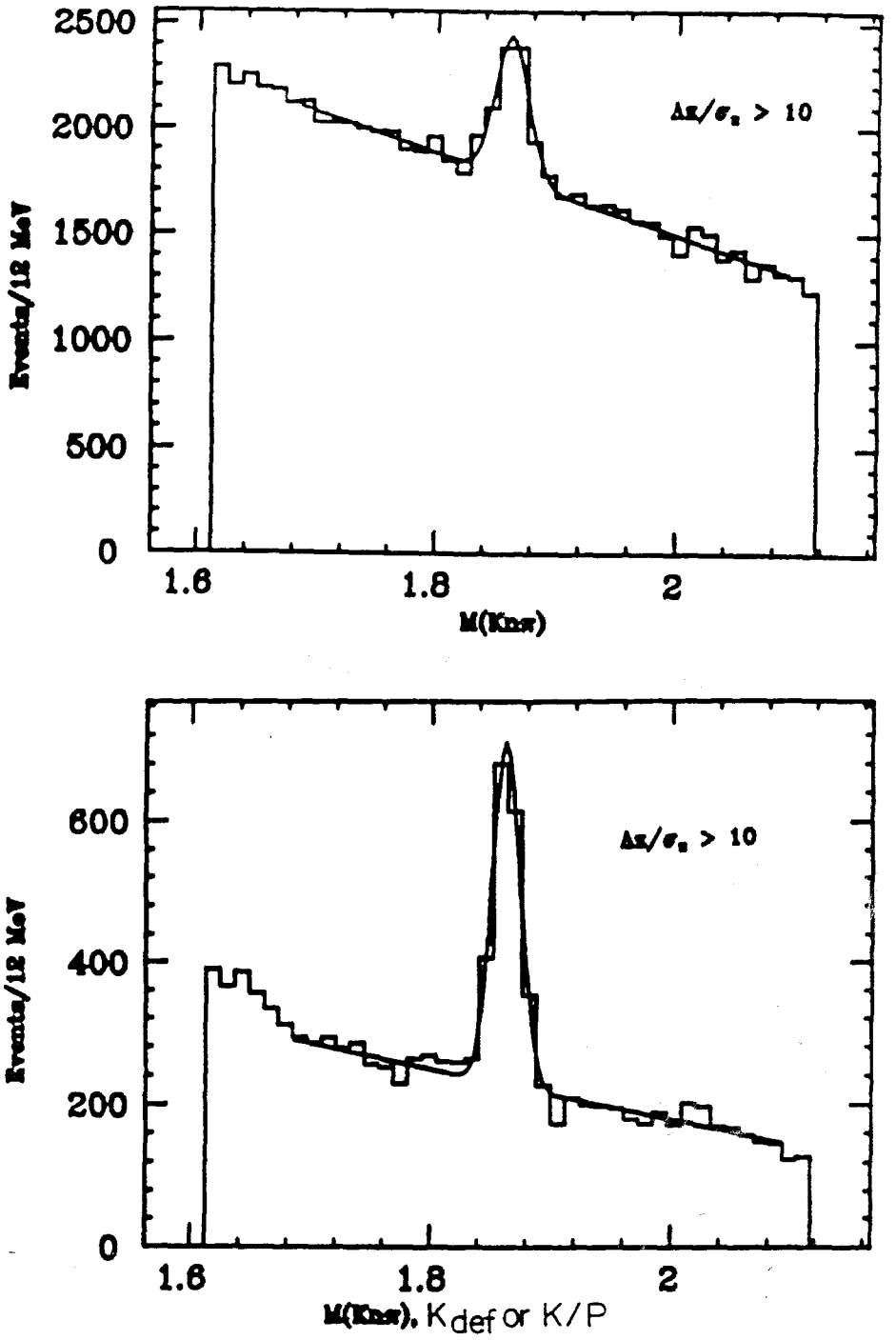

Figure 17: Performance of Cerenkov counters

tend to increase confusion in tightly clustered events. In addition, adding more radiator will increase the P0 $\rightarrow$ P2 lever arm by 12 % which will cause a small decrease in our total acceptance.

4.2 Electromagnetic calorimeters

4.2.1 Inner electromagnetic calorimeter

The Inner Electromagnetic Calorimeter or IE is a 25 radiation length lead-scintillator sandwich calorimeter which is used to identify electrons and photons. The device is divided into 3 longitudinal modules and is readout by X and Y strips. In order to match X and Y fiber strips that are "hit", there are two additional 45 degree scintillator arrays called tiebreakers.

Thus far we have used the device to reconstruct semileptonic decays to electrons and have identified many charm channels containing π^0's. The efficiency for identifying electrons hitting the inner electromagnetic calorimeter is approximately 90% with a e/π rejection ratio of 1/50. This efficiency can be improved, but then we have more pion contamination. However, the efficiency is quite acceptable. Our photon reconstruction efficiency for photons striking the IE calorimeter is between 50% and 60%. This low efficiency is partly due hadronic showers overlapping photonic showers and partly due to the tiebreaker matching. We are presently investigating replacing the tiebreakers with a single layer of tiles 7.5cm $\times$ 7.5cm $\times$ 2cm thick. A total of 480 tiles would be required. By removing the tiebreakers we would save 156 channels such that an additional 324 new channels would need to be obtained. While this design needs to be further studied in Monte Carlo, it appears that we may be able to double the number of π^0's reconstructed in the IE with such an addition.

Finally, we need to create an E_{perp} trigger from energy which is deposited in the IE. We presently plan to implement such a trigger by weighting the pulse heights from the X and Y strips in the middle longitudinally segmented module by the distance the strips are away from the beam direction. The phototubes have dynode outputs which were designed for such a plan.

4.2.2 Outer electromagnetic calorimeter

The E687 OE is a lead-scintillator sandwich calorimeter, with active media readout done with fine-grained (3.3 cm) strips, covering the wide-angle region (from $\sim 40\,mrad$ up to $\sim 120\,mrad$). The two halves of the detector are separated by an adjustable gap with respect to the magnet bend plane (in E687 set to 9 cm), therefore the pile-up due to pairs will be easily kept under control.

Two upgrades are considered for this detector. The inner part of the detector will be modified in order to improve the shower reconstruction efficiency in the highest occupancy region, i.e. in the region close to the hole where X-Y strips matching is most problematic. The second upgrade will consist in inserting the OE information in the second level triggering logic.

The inner region will be replaced by a monolithic detector made of plastic scintillating fibers embedded in a lead matrix with a 50:35 scintillator-to-lead volumic ratio, fibers parallel to the beam axis and tower-like readout. This *head-on* technique has been used in the $(20\,MeV - 5\,GeV)$ energy range attaining $6\%/\sqrt{E[GeV]}$ energy resolution [37, 38]. Prototyping and testing have been performed in Frascati. The upgraded region will consist of two monolithic Pb-scintillating fibers structures, each one symmetric to the magnet bending plane, running along the vertical gap and the central hole with a 25 cm width in the (X,Y) plane and 32 cm $(20X_o)$ thickness. Each structure is made of grooved lead foils (1.3 mm thickness) and 1mm-diameter scintillating fibers. During the assembly, fibers are pre-cut to measure and positioned in a transport frame which allows to stack and glue lead foils together. Once assembled, fibers are uniformly positioned throughout the lead volume forming a periodical hexagonal lattice. The interaxial distance from each fiber to its closest neighbours is 1.35 mm. Such an inner region in addition will improve both energy and spatial resolution for photons. More than 90% of the photon pairs from π^o in charm decays in the OE angular acceptance are wider than 10cm. The present design sees a $(5 \times 5)\,cm^2$ readout granularity leading to 240 counters in total.

The strip-like structure of the readout elements permits to design an E_{perp} fast trigger based on thresholds varying with the distance from the beam axis. Before being converted, a small fraction of the counters' signal is picked-up and sent to a low-threshold discriminator. Such front-end electronics has been prototyped and tested, about 500 channels are available.

5 Computing Requirements

The event reconstruction of the data for the present run of E687 is now complete. It required about 600 VAX/780-years. This was accomplished in 10 months using UNIX farms. Since the data-set anticipated for the 1993-1994 run is 5 times larger, it is reasonable to estimate a requirement of 4500 VAX/780-years. We use a factor of 7.5 rather than 5 because the trigger will preferentially eliminate the lowest multiplicity, simplest events. This amount of computing should be readily available at affordable prices by 1994/5, when it would be needed. However, we anticipate reducing computer use by approximately a factor of two by not performing the whole analysis on every event. One possible strategy would be to perform all the track reconstruction and fast particle identification algorithms ($< 40\%$ of the present offline analysis package) and only further analyze those events with evidence for a secondary vertex, or unusual final state particles (e.g. multiple kaons and protons and/or leptons). From our **present analysis**, we estimate that less than 20% of the events will survive these selection criteria. (We have previously skimmed with an algorithm that selected 10% of the events while still being 80% efficient for reconstructable charm decays.) Extensive hadron and electromagnetic calorimetry analysis would only be performed for the skimmed events. This should result in a requirement of less than 1500 Vax years. If one takes the point of view that 900 additional VAX/780-years will need to be acquired for this experiment, then, assuming \$50/VUP by 1994/5 (as compared to \$118/VUP in FNAL's last acquisition), the incremental cost of the computing is \$45,000. It should be noted that the proposed gains come from doing less analysis on events which are already believed to be uninteresting, not by doing a less-than-complete microstrip or spectrometer tracking. We will, of course, investigate whether partial tracking can further reduce the CPU requirement.

During E687, it was possible to analyze about 25% of the events during data taking. We hope to have the analysis ready at the start of E831 so we would like to have the full reconstruction capacity available from the beginning of the run to keep up with data-taking.

6 Beam Request and Running Conditions

6.1 Beam Request

We can most realistically formulate our beam request by scaling from the 1990/92 runs. This will fold in the effects of real-life problems that occur during data-taking.

In 1990/91, we accumulated about 15 million events per week and got an effective 35 weeks of data. If we had sustained the optimum running conditions for the experiment, we would have accumulated about 28 milliion events/week. There was very little down time from malfunctioning of experimental equipment. The difference between the optimum and the reality was due to accelerator and beam downtime, 'edge effects' such as tuning and beam instabilities, low machine intensity, and, to some extent, time needed for calibration. In the 1991 run, calibration time was especially long because of the presence of E683 which needed separate beam calibration time. In addition, in 1991, E683's running condition limited the beam intensity to 3E12 when E687 could easily have taken 4 or 5E12. In the two runs, we were charged for about 5000 beam hours.

We therefore request a running period of 1000 beam hours for setup and 4000 beam hours for data-taking. The 1000 hours represents more than was required for either the 1990 or 1991 startup. However, we will have many new components that will have to be calibrated and we will have to learn their idiosyncracies. We will also have to learn how to run at the higher rates. When we brought the experiment up for the first time, in 1987/88, it took us about 1000 hours to get everything working and the trigger understood.

Our desired running conditions are 900 GeV/c proton beam with 5E12 protons on target. The rep rate should be about 1 spill/minute. The flat top should be at least 20 seconds. Intensities during tuneup can be lower, beginning at 2E12.

We expect to operate the secondary beam in double band mode. We need to use the liquid deuterium production target to achieve the required photon yield. Other modifications to the beam have been described above.

We strongly prefer a single Fixed Target running period to complete the above goals.

6.2 Special Considerations

This experiment will be much more sensitive to spill structure than our previous efforts. We would strongly urge the lab to fold standard spill quality monitoring, feedback, and spill improvement into its plans for the upcoming fixed target run. We believe the average 'coarse spill duty factor' of around 40-50% should be improved to at least 80%, a number that has been achieved under some circumstances. We believe that additional attention should be devoted to studying and improving the spill 'micro-structure'– bucket to bucket correlations,etc.

References

[1] I. Bigi,$D^0\bar{D}^0$ Mixing and CP Violation in D Decays- Can There Be High Impact Physics in Charm Decays?, Tau-Charm Factory Workshop,SLAC,Stanford,May,1989

[2] A. Datta and D. Kumbhakar,Z.Phys.C,27(1985),515

[3] Lincoln Wolfenstein,Phys. Lett.,164B,(1985)170

[4] P. Colangelo,G. Nardulli, and N. Paver, Phys. Lett. B, 242(1990)71

[5] N. Isgur and M. B. Wise, Weak Decays of Heavy Mesons in the Static Quark Approximation,Phys. Lett,232B,113,1989

[6] Sheldon Stone, HEPSY preprint 1-92, April 1992

[7] H. Abramowicz *et al.*, *Z.Phys. C* **15**, 19(1982)

[8] Joseph M. Izen, "Semileptonic Charm Decay at a Tau Charm Factory", contributed to SLAC-Report-343, June 1989, pp. 605-615.

[9] R.M. Baltrusaitis *et al.*, *Phys. Rev. Lett.* **54**, 1976(1985)

[10] R.M. Baltrusaitis *et al.*, *Phys. Rev. Lett.* **66** 142(1991)

[11] K. Kodama *et al.*, *Phys. Rev. Lett.* **66** 1819(1991)

[12] G. Crawford *et al.*, *Phys. Rev.* **D44** 3394(1991)

[13] J.C. Anjos *et al.*, *Phys. Rev. Lett.* **62**, 1587(1989)

[14] J. Adler *et al.*, *Phys. Rev. Lett.* **62**, 1821(1989)

[15] J. Adler *et al.*, *Phys. Rev. Lett.* **60**, 89(1988)

[16] J.R. Raab *et al.*, *Phys. Rev.* **D37**, 2391(1988)

[17] J.C. Anjos *et al. Phys. Rev. Lett.* **62**, 1717(1989)

[18] P. Avery *et al. Phys. Rev.* **D41**, 774(1990)

[19] H. Albrecht *et al. Phys. Lett.* **B232**, 398(1989)

[20] H. Albrecht *et al. Phys. Lett.* **B231**, 422(1989)

[21] H. Albrecht *et al. Phys. Lett.* **B231**, 208(1989)

[22] H. Albrecht *et al. Phys. Lett.* **B230**, 162(1989)

[23] M.B. Voloshin and M.A. Shifman, ZH. Eksp. Teor.Fiz. 91,1180 (1986) and B. Guberina *et.al.*, Z.Phys **C33**,297 (1983).

[24] This is actually the ratio of the $\tilde{\pi}$ energy in the D^{*+} rest frame to the D^{*+} mass. Fluctuations in this energy ratio due to the finite energy release, Q, implies a roughly $\pm$ 16% measurement of the parent D^{*+} momentum can be obtained by rescaling the $\tilde{\pi}$ momentum by a factor of 13.8.

[25] See Figure13 for the charm-anticharm P_t balance observed in a sample of $\approx$ 200 fully reconstructed D and $\overline{D}$ obtained during the 1990 run of E687.

[26] M. Mangano, P. Nason and G. Ridolfi, Nucl. Phys. B 373 (1992) 295.

[27] *Studies of Fully Reconstructed $D\overline{D}$ Events in High Energy Photoproduction*, Contributed paper to the *XXVI International Conference on High Energy Physics*, Dallas TX (USA), August 6-12, 1992; by Rob Gardner for the Fermilab E687 Collaboration.

[28] NA14 Collab., M.P. Alvarez *et al.*, Phys. Lett. B 278 (1992) 385.

[29] For the case of D^o recoil candidates, we first remove any primary vertex tracks consistent with forming a D^{*+} with the *recoil* D^o by eliminating tracks within $\pm$3 MeV of the known $D^* - D$ mass difference. Such tracks create a significant wrong sign background to the $\tilde{\pi}$ sample.

[30] G. Jaross, PhD thesis, *Photoproduction of $D^{*\pm}$ and D^o Mesons* , University of Illinois at Champaign-Urbana (1991), page 118

[31] *Measurement of the Branching Ratio* $\Gamma(D^0 \rightarrow K^-\mu^+\nu)/\Gamma(D^0 \rightarrow K^-\pi^+)$, Contributed paper to the *XXVI International Conference on High Energy Physics*, Dallas TX (USA), August 6-12, 1992; by Gianpaolo Bellini for the Fermilab E687 Collaboration.

[32] I.I. Bigi "CP Violation in D Decays", p169-195, Tau-charm Factory Workshop,SLAC,Stanford, May 23-27,1989
and Ling-Lie Chau "CP Noninvariance: A Charm Possibility" p695-705, Tau-charm Factory Workshop,SLAC,Stanford, May 23-27,1989

[33] M. Golden and G. Grinstein, Phys. Lett. **B222**, 501 (198 9);
K.Kleinknecht and B. Renk,*Z.Phys. C* **34**, 209(1987).

[34] A. Datta *Phys. Lett.* **B154** 170(1985)

[35] E.D. Commins and P.H. Bucksbaum, "Weak Interactions of Leptons and Quarks", Cambridge University Press (1983)

[36] I.I. Bigi and A.F. Sanda, *Phys. Lett.* **B171** 320(1985)

[37] D.W. Hertzog *et al., Nucl. Instr. and Meth.* **A294**, (1990) 446-459.

[38] S. Bianco *et al, Nucl. Instr. and Meth.* **A315**, (1992) 322-326.

[39] The E687 Collaboration, Description and Performance of the Fermilab E687 Spectrometer, FERMILAB-Pub-90/258-E (1990). Section 2.2 describes the Beam Tagging System and Beam Gamma Monitor for the 1987-88 running period and due to space considerations was not included in the article accepted for publication in NIM.

[40] G. Alimonti, et al., Nucl. Instr. and Meth. **A314**(1992)411.

[41] Karen Lingel, Ph.D. thesis, U. of Illinois, 1990;
Hector Mendez, Ph.D. thesis, U. of Mexico, 1990;
R. Yoshida, Nucl. Instr. and Meth. **A302**(1991)63.

[42] J. Knauer, et al., Some Photon and Neutron Calorimeters for FNAL Experiment 87, Proc. Calorimeter Workshop, Fermilab, 1975, page 215.